Chem Soc Rev

REVIEW ARTICLE

View Article Online
View Journal | View Issue

Cite this: *Chem. Soc. Rev.*, 2022, **51**, 4763

The integration of bio-catalysis and electrocatalysis to produce fuels and chemicals from carbon dioxide

Xinyi Tan[a] and Jens Nielsen *[bc]

The dependence on fossil fuels has caused excessive emissions of greenhouse gases (GHGs), leading to climate changes and global warming. Even though the expansion of electricity generation will enable a wider use of electric vehicles, biotechnology represents an attractive route for producing high-density liquid transportation fuels that can reduce GHG emissions from jets, long-haul trucks and ships. Furthermore, to achieve immediate alleviation of the current environmental situation, besides reducing carbon footprint it is urgent to develop technologies that transform atmospheric CO_2 into fossil fuel replacements. The integration of bio-catalysis and electrocatalysis (bio-electrocatalysis) provides such a promising avenue to convert CO_2 into fuels and chemicals with high-chain lengths. Following an overview of different mechanisms that can be used for CO_2 fixation, we will discuss crucial factors for electrocatalysis with a special highlight on the improvement of electron-transfer kinetics, multi-dimensional electrocatalysts and their hybrids, electrolyser configurations, and the integration of electrocatalysis and bio-catalysis. Finally, we prospect key advantages and challenges of bio-electrocatalysis, and end with a discussion of future research directions.

Received 20th April 2022

DOI: 10.1039/d2cs00309k

rsc.li/chem-soc-rev

1. Introduction

Fossil fuels assume a key position in human society. However, the total amount of fossil fuels on earth is limited, and it is crucial to find substitutes and sustainable energy sources to replace them in the future. Furthermore, the dependence on

[a] *Department of Materials Science and Engineering, Beijing Institute of Technology, Beijing, 100081, China. E-mail: monica950521@126.com*
[b] *Department of Biology and Biological Engineering, Chalmers University of Technology, SE41296 Gothenburg, Sweden. E-mail: nielsenj@chalmers.se*
[c] *BioInnovation Institute, Ole Maaløes Vej 3, DK2200 Copenhagen N, Denmark*

Xinyi Tan

Xinyi Tan received her PhD degree in Chemical and Biomolecular Engineering of University of California Los Angeles (UCLA), where she had an in-depth study of energy storage materials for lithium-ion and sodium-ion batteries. Tan received her bachelor degree in polymer materials and engineering in Jilin University. Now she is a post doc in Materials Science and Engineering of Beijing Institute of Technology, and focused on the research of energy storage and CO_2 reduction that based on the integration of electrocatalysis and bio-catalysis.

Jens Nielsen

Jens Nielsen is a professor at Chalmers University of Technology, Sweden, and CEO of the BioInnovation Institute in Denmark. Prof. Nielsen is member of several academies, including the National Academy of Engineering and National Academy of Science in USA, Chinese Academy of Engineering, the Royal Swedish Academy of Science, the Royal Danish Academy of Science and Letters, and the Royal Swedish Academy of Engineering Sciences. Prof. Nielsen has published so far more than 850 papers that have been cited more than 90 000 times (current H-factor 134), and co-authored more than 40 books. He has received numerous awards, including the ENI Award for new energy solutions.

fossil fuels has caused excessive emissions of greenhouse gases, intensifying the risk of climate change and global warming. To circumvent these severe consequences and avoid the point of no return, ''2-degree scenario'' should be met. It requires that increases in global temperature are less than 2 °C above 'pre-industrial' levels. Major efforts have been directed towards the capture and utilization of CO_2. However, capture and storage of CO_2 (mostly underground) is energy intensive, cost prohibitive, and incapable of producing value-added compounds. Transformation of CO_2 as cheap, nontoxic, and naturally abundant carbon-based resource into fuels and chemicals is desirable from both ecological and economic viewpoints, and is therefore attractive.

Current CO_2 utilization approaches include photocatalysis, chemical catalysis, bio-catalysis and electrocatalysis.[1] Among these strategies, electrocatalysis is particularly appealing because it simply makes use of clean and renewable electricity (with lower costs deriving from growing abundant sources) generated at (or near) room temperature and ambient pressure, enabling a sustainable future with a low-carbon footprint. During this process, the required hydrogen is generated *in situ* by water electrolysis, thus eliminating the use of blue hydrogen from fossil fuels. The application of electrocatalysis is suitable to decentralization and holds great economic promise with a foreseen surplus of cheap electrical energy from a well-distributed and intermittent renewable source that would otherwise be difficult to store. Nevertheless, it remains a challenge to obtain long-chain carbon products with high selectivity *via* direct CO_2 electrocatalysis, due to the high C–C coupling energy barrier, the linear scaling relations, as well as the concurrent occurrence of the competing hydrogen evolution reaction (HER).

Considering that bio-catalysis can produce a wide range of C_{2+} products (containing two or more carbon atoms) with high efficiency and specificity, the integration of bio-catalysis with electrocatalysis through rational design of electrode and catalyst materials using CO_2 and renewably generated electricity has spurred increased research interest. Classic electrocatalysis for CO_2 fixation is efficient in many ways, however, the most feasible products remain CO, methane, methanol and formic acid, while ethanol and other C_{2+} chemicals are difficult to obtain.[2] In addition, there are different catalytic pathways for CO_2 reduction leading to multiple compounds at similar overpotentials, which affects the selectivity of the reaction.[3] By combining advantages of both bio-catalysis and electrocatalysis, bio-electrocatalysis aims to produce C_{2+} products from CO_2 with high conversion efficiency and selectivity.[4,5]

Great achievements have been made in bio-electrocatalysis. For example, the cost of electricity from renewable sources has reduced substantially.[6] Advanced devices, complex three-dimensional electrode materials and their hybrids have been developed to enhance the electron transfer efficiency and the CO_2 utilization rate.[7,8] Furthermore, the suitable candidates for electrocatalysis have been identified, involving efficient C1 utilizing enzymes, pathways and microbial cell factories,[9,10] as demonstrated by the production and commercialization of several C_{2+} products.[11–13] In this review, we first provide a fundamental explanation of CO_2 utilizing classic electrocatalysis and bio-electrocatalysis. Next, key aspects for bio-electrocatalysis are discussed. A summary of the most important advances in the design of electron transfer materials, catalysts, electrolytes, electrolysers, promising CO_2 fixation and pathways, as well as compelling microbial hosts is presented. Strategies to further boost the integration of bio-catalysis and CO_2 electrocatalysis are highlighted. Finally, future challenges and prospects of CO_2 conversion *via* coupling of bio-catalysis and electrocatalysis are outlined.

2. Electrocatalysis-based CO_2 reduction

CO_2 transformation cannot be carried out spontaneously due to thermodynamic constraints, and external energy is required to drive the reduction. Many efforts have been attempted to elucidate the mechanisms of CO_2 reduction in both theoretical and experimental research. However, due to the complexity of these pathways and difficulties in capturing intermediates of the reactions, many of the molecular mechanisms have only been confirmed partially for a few steps. The transfer of electrons and protons provides the driving force for CO_2 reductions. Various products such as CO, formic acid, methane, methanol, ethylene, ethanol, and other hydrocarbons can be acquired, and different numbers of electrons and protons are transferred to carbon dioxide. Equations 1–10 display the Gibbs free energy (at 298 K, 1 atm) and the reduction potential *versus* standard hydrogen electrode (SHE) at pH = 7 of various CO_2 reduction reactions with different products.[14] Gibbs free energies for all these reactions are higher than zero, suggesting that they cannot take place without external energy input. It is obvious that long-chain carbon products require more energy input to proceed the reactions and therefore are harder to produce than C1 chemicals. In electrocatalysis-based CO_2 reduction, electricity that is generated by renewable energy can be introduced as the driving force, and catalysts that can reduce energy barriers during the reactions can achieve high conversion efficiency for the products. Due to the clean and sustainable energy source of CO_2 electrocatalysis and the high selectivity for long-chain carbon products of bio-catalysis, the integration of electrocatalysis and bio-catalysis can combine the merits of both transformations.

2.1 Classic electrocatalysis for CO_2 reduction

During classic electrocatalysis for CO_2 reduction, electrons and protons that participate in reactions usually derive from the electrolytes (Fig. 1a).[15] Dispersed CO_2 gas will first dissolve in the electrolyte solution and then adsorbed by binding sites or defects on the surface of catalysts to form a CO_2^{*-} radical anion. The CO_2^{*-} has short lifetime and is rapidly protonated to either form *COOH or *OCHO. After the second electron transfer and protonation, *COOH is reduced to CO*, which are key intermediates in forming hydrocarbons or oxygenates in CO_2 electroreduction. For example, the CO* intermediate can form

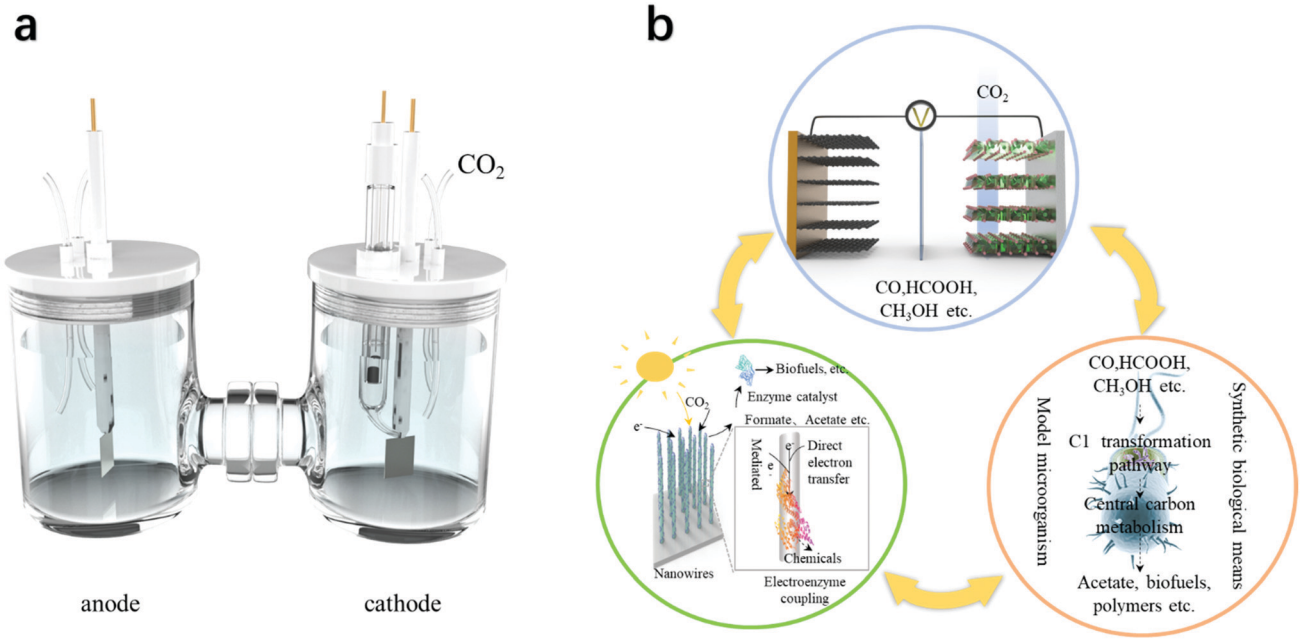

Fig. 1 The two generations of electrocatalysis used for CO_2 conversion. (a) Classic electrocatalysis that utilizes electricity to produce mainly C_1 and C_2 compounds. (b) Bio-electrocatalysis that could efficiently utilize electricity from renewable sources together with bio-catalysis to produce C_{2+} compounds.

COH* or CHO* through electron-proton pair transfer, and these two intermediates can be reduced to methanol in subsequent steps. During the formation of C_2 compounds, the C–C bond is coupled between surface-bound C_1 oxygenates, through enol-like surface species to other C_2 compounds with further oxidation-reduction reaction. Classic electrocatalysis of CO_2 can occur through these reactions and produce various products, including formic acid, CO, methanol, methane, ethanol, and ethylene.[16,17] However, their most feasible products remain C_1 products, with C_{2+} chemicals being difficult to produce.

$$CO_2 + 2H^+ + 2e^- \rightarrow CO + H_2O, \quad \Delta G^\circ = 102.274 \text{ kJ mol}^{-1}, \quad E^{\circ\prime} \text{ redox} = -0.53 \text{ V} \quad (1)$$

$$CO_2 + 2H^+ + 2e^- \rightarrow HCOOH, \quad \Delta G^\circ = 117.712 \text{ kJ mol}^{-1}, \quad E^{\circ\prime} \text{ redox} = -0.61 \text{ V} \quad (2)$$

$$2CO_2 + 2H^+ + 2e^- \rightarrow H_2C_2O_4, \quad \Delta G^\circ = 176.182 \text{ kJ mol}^{-1}, \quad E^{\circ\prime} \text{ redox} = -0.91 \text{ V} \quad (3)$$

$$CO_2 + 4H^+ + 4e^- \rightarrow HCHO + H_2O, \quad \Delta G^\circ = 185.251 \text{ kJ mol}^{-1}, \quad E^{\circ\prime} \text{ redox} = -0.48 \text{ V} \quad (4)$$

$$CO_2 + 6H^+ + 6e^- \rightarrow CH_3OH + H_2O, \quad \Delta G^\circ = 219.986 \text{ kJ mol}^{-1}, \quad E^{\circ\prime} \text{ redox} = -0.38 \text{ V} \quad (5)$$

$$CO_2 + 8H^+ + 8e^- \rightarrow CH_4 + 2H_2O, \quad \Delta G^\circ = 185.251 \text{ kJ mol}^{-1}, \quad E^{\circ\prime} \text{ redox} = -0.24 \text{ V} \quad (6)$$

$$2CO_2 + 12H^+ + 12e^- \rightarrow CH_2H_4 + 4H_2O, \quad \Delta G^\circ = 404.079 \text{ kJ mol}^{-1}, \quad E^{\circ\prime} \text{ redox} = -0.35 \text{ V} \quad (7)$$

$$2CO_2 + 12H^+ + 12e^- \rightarrow C_2H_5OH + 3H_2O, \quad \Delta G^\circ = 380.923 \text{ kJ mol}^{-1}, \quad E^{\circ\prime} \text{ redox} = -0.33 \text{ V} \quad (8)$$

$$2CO_2 + 14H^+ + 14e^- \rightarrow C_2H_6 + 4H_2O, \quad \Delta G^\circ = 364.713 \text{ kJ mol}^{-1}, \quad E^{\circ\prime} \text{ redox} = -0.27 \text{ V} \quad (9)$$

$$3CO_2 + 18H^+ + 18e^- \rightarrow C_3H_7OH + H_2O, \quad \Delta G^\circ = 538.386 \text{ kJ mol}^{-1}, \quad E^{\circ\prime} \text{ redox} = -0.31 \text{ V} \quad (10)$$

2.2 Volcano plot and scaling relationship

Nobel laureate Paul Sabatier stated that an "ideal" catalyst should interact with a substrate neither too weak (*i.e.*, strong binding of reactants) nor too strong (*i.e.*, weak binding of products ensuring their desorption at ease), which is known as the Sabatier's principle. A too strong binding strength leads to surface poisoning, while a too weak adsorption entails insufficient coverage and thus poor reaction rate. Plotting the catalytic performance against the binding energy of reactants yields a "volcano" plot.[18] This can be used as an intuitive tool to compare the thermodynamics among catalysts, assisting understanding and predicting active candidates that may approach the peak or plateau of the volcano. The volcano slopes indicate regions where the catalyst/intermediates binding is either too strong (left slope) or too weak (right slope).[18] For CO_2 reduction reactions, the crucial intermediate for the volcano plot varies according to the type of product.

Given that analogous surface–C bonds are formed regardless of different CO_2 reduction intermediates (*e.g.*, *CO, *COOH, and *COH, * denotes the adsorbed site), it remains a formidable challenge to optimize the binding strength of the key

intermediate without impacting the other products. This phenomenon is referred to as scaling relationship. As a proof-of-principle example, the hydrogenation of *CO to *CHO is inferred to be the potential-determining step (PDS) of CO_2 reduction to CH_4.[19] The high free energy change of this step (0.74 eV) is plausibly attributed to the weak adsorption of *CHO as opposed to *CO. However, achieving stronger binding of *CHO (*i.e.*, more negative) than *CO for selective CH_4 formation is limited by the scaling relationship.[20] By analogy, the weak binding of *COOH caused by the linear scaling between *COOH and *CO results in large overpotentials and low turnover frequencies of Ag and Au electrodes for CO_2 conversion to CO.[21] Conceptually resembling the general scaling relationships delineated in heterogeneous catalysts, a decrease in thermodynamic effective overpotential η_{eff} (the difference between redox potential of a molecular catalyst and the thermodynamic CO_2 reduction potential) is usually correlated with drop in the kinetic maximum catalytic turnover frequency TOF_{max} (as reflected by the plateaued catalytic current) for molecular catalysts. This general trend is often described as a "molecular scaling relationship" (*i.e.*, the trade-off between η_{eff} and TOF_{max}). From these scenarios, optimization of the binding energy of a specific intermediate by overcoming the energetic linearity constrains enables one to lower the overpotential and improve selectivity. To this end, several useful protocols based on alloying, tethering active ligands, introducing promoters, and creating multiple functional sites may be attempted.[22] Exploration of mixed solvents may be another avenue.

2.3 Competition between CO_2 reduction and hydrogen evolution

CO_2 activation and reduction process is always plagued by the concomitant HER (from proton and/or water reduction) in protic solvents. HER has a much faster kinetics and proceeds at a similar or even more positive potential compared with the CO_2 reductions. Meanwhile, the simultaneous binding of *H with CO_2 reduction intermediates influences their adsorption energies, thus profoundly affecting reaction kinetics. Therefore, to boost the CO_2 reductions, parameters such as the properties of electrode, local availability of protons/water, operating conditions, and composition of electrolyte can be tailored to combat the undesired HER. This can be done by (1) using an electrolyte with diminished proton donor activity (*e.g.* organic solvents with a low dissociation constant, ionic liquids, and mixed solvents);[23] (2) optimizing reaction conditions (with comparatively lower local alkalinity near the electrode surface and enhanced mass transport);[24] (3) engineering electrode-electrolyte interface to construct aprotic and hydrophobic protection layers;[25] or by (4) modifying electrocatalysts to favour adsorption and binding of CO_2 rather than hydrogen.[26]

2.4 Bio-electrocatalysis for CO_2 reduction

Bio-electrocatalysis employs biocatalysts to enhance the productivity and selectivity in production of C_{2+} products, and can be divided into enzymatic electrocatalysis and microbial electrocatalysis (Fig. 1b). Classic electrocatalysis is characterized by high electron transfer efficiency, while bio-catalysis has the ability to produce more valuable and complex products with high specificity, stereoselectivity and regioselectivity.[27] Moreover, biocatalysts including oxidoreductases and microbes that can utilize C_1 and C_2 substrates are diverse and abundant. By using substrates produced through classic electrocatalysis, bio-electrocatalysis has the potential to produce a wide range of C_{2+} fuels and chemicals.[28] Microbes used in bio-catalysis could also be considered as self-regenerating catalysts with long-term stability, and sustainability.[29] Bio-electrocatalysis can be divided into direct-electron-transfer strategies and indirect-electron-transfer strategies. During direct-electron-transfer bio-electrocatalysis, electrocatalysis and bio-catalysis could be carried out in one pot, and electrons generated from renewable sources can be consumed by biocatalysts directly or indirectly through electron carriers, such as hydrogen, ammonia, sulphur species and ferrous salts, to convert CO_2 into desired products.[30,31] During indirect-electron-transfer bio-electrocatalysis, CO_2 is first converted into C_1 and C_2 compounds through classic electrocatalysis. These C_1 and C_2 compounds can then be used as substrates, mostly in separate devices, for biocatalysts to produce desired products with higher chain lengths. Formate dehydrogenase (FDH),[29] formaldehyde dehydrogenase (FaldDH),[32] acetogens,[33] methanogens,[34,35] *Clostridia*,[36] and other biocatalysts capable of efficiently utilizing C_1 and C_2 compounds can be used in indirect-electron-transfer strategies, and a wide range of chemicals including secondary metabolites can hereby be produced.

3. Crucial factors in bio-electrocatalysis

Bio-electrocatalysis aims to improve product range and efficiency through interlinking classic electrocatalysis with biocatalysis. Crucial factors in bio-electrocatalysis include electron transfer materials, catalysts, electron transfer and catalytical materials complexes with one-dimensional, two-dimensional, or three-dimensional composites, electrolyser configurations, as well as promising CO_2 fixation pathways and attractive microbial hosts.

3.1 Electron transfer materials

Electron transfer materials are used to transport and conduct electrical currents. Electron transfer materials include metals, semi-conductors, carbon-based materials, metal-organic frameworks (MOFs) and other composites. Key factors that govern the performance of electron transfer materials are Ohmic resistance, concentration polarization potential and the driving force required by the reaction itself. A good electron transfer material should have small Ohmic resistance and low concentration polarization potential. Silver, copper, gold, and platinum are typical metal materials with good electrical conductivity, while silicon and germanium are representative materials in the family of semi-conductors. Detailed information of metal and semiconductor materials can be found in recent reviews.[37,38]

Carbon-based materials are divided into several categories, such as carbon nanotubes, graphene, and reduced graphene

oxide. Carbon nanotubes (CNTs) are composed by carbon hexagons that are arranged in a concentric manner.[39] CNTs are widely used by catalysis due to their high specific area (1315 $m^2 g^{-1}$ for single-walled CNTs),[40] extraordinary electrical conductivity (5000 S cm^{-1}) and high chemical stability.[41] As the most common one-dimensional material with outstanding electrical conductivity, CNTs can be utilized as the electron transfer to mediate and support catalytically active sites during the CO_2 transformation process.[42,43] For example, Wu *et al.* reported the utilization of N-doped CNTs in CO_2 electrocatalysis and obtained CO as the major product with faradaic efficiency of 80% at −0.78 V *vs.* RHE (reversible hydrogen electrode).[44] The defects in N-doped CNTs can provide more catalytically active sites for CO_2 reduction, and lead to a lower free energy barrier for the adsorption of COOH which is a potential rate-limiting step in CO formation. In addition, the pyrrolic-N and pyridinic-N in N-doped CNTs can also enable favourable CO desorption with suitable binding energy that can be beneficial to CO production.

Another typical carbon-based material is graphene, with large specific surface area (2630 $m^2 g^{-1}$), good thermal conductivity (5000 W $m^{-1} K^{-1}$), high electrical conductivity (106 S cm^{-1}) and high mechanical strength.[45,46] Han *et al.* described a defective graphene that can be used in CO_2 electrocatalysis to acquire CO as the major products with a faradaic efficiency of 84% at −0.6 V *vs.* RHE, the topological defects in graphene can expose abundant catalytically active sites for CO_2 reduction and provide strong adsorption capacity for CO_2 which can improve the conversion efficiency for reduction products.[47] Chae *et al.* compared different types of composite materials, and managed to produce 40.6% methane using the Ni nanoparticles doped granular activated carbon composite.[48] The granular activated carbon with large surface area can function as a conductive bridge to transfer electrons and protons between different microbes and provide multiple catalytically active sites, and Ni catalysts in the composites exhibit high catalytic activity and low toxicity to microbes that can be favourable in methanogenesis.

MOFs are also attractive materials with diverse structures and stable porosity.[49] The specific framework formed by metal and organic coordination not only has metal activity, but also obtain the flexibility of organic ligands, the selectivity of functional groups, the special spatial structure, and other physical and chemical properties from organic coordination at the same time.[50] The porous structure of MOFs can provide a large amount of catalytically active sites and immense pore volume to accommodate CO_2 molecules which has a significant influence on the improvement of conversion efficiency of CO_2 reduction.[51,52] Deng *et al.* employed bismuth-based MOFs to fabricate Bi_2O_3@C-800 composites to achieve formate production with a 92% faradaic efficiency and a partial current density of 7.5 mA cm^{-2} at −0.9 V *vs.* RHE in CO_2 electroreduction, the MOFs in the composites act as a carbon matrix with high electrical conductivity and abundant adsorption sites for CO_2, while Bi_2O_3 contributes to the high selectivity and conversion efficiency of formate during the electroreduction.[53] Qiu *et al.* reported MOFs composites PcCu–Cu–O which can transform

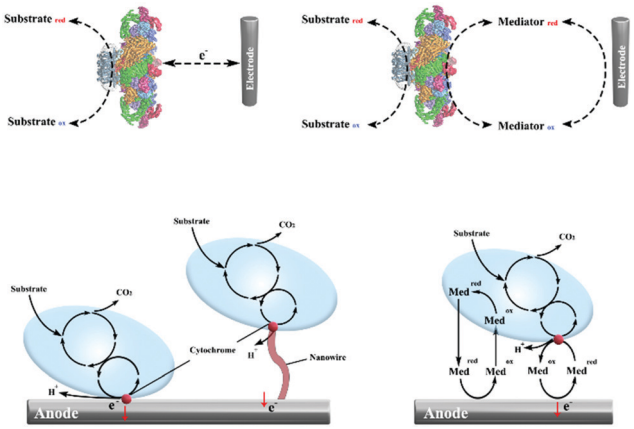

Fig. 2 Schemes of DET and MET in enzymatic electrocatalysis and microbial electrocatalysis. (a) DET in enzymatic electrocatalysis. (b) MET in enzymatic electrocatalysis. (c) DET in microbial electrocatalysis. (d) MET in microbial electrocatalysis.

CO_2 into C_2H_4 with a faradaic efficiency of 50%, and it has been shown that the abundant C_2H_4-producing and CO-producing sites in this MOFs composites can be favourable in C_2H_4 formation, and the high crystallinity and strong π–π interaction between MOFs layers can be helpful in limiting the distortion of Cu ions from tetragonal to tetrahedral which guarantee the electrode durability for electro-conversion of CO_2 to C_2H_4.[54]

Different from the traditional electron transfer materials in CO_2 electroreduction, cofactors such as NAD/$NADH^+$, ATP/ADP, $FMNH_2$/$FADH_2$ serve as typical electron transfer media in biocatalytic reduction of CO_2.[55,56] Cofactors can provide protons and electrons during the oxidation–reduction process in microbial systems, and enzymes function as catalysts in the biocatalysis process. Eelectron transfer in enzymatic and microbial electrocatalysis can be divided into a direct electron transfer (DET) scheme and a mediated electron transfer (MET) scheme (Fig. 2).[57–59] During DET schemes, electrons could be utilized directly by oxidoreductase containing active centres and microbes through membrane-bound redox proteins.[60] During MET schemes, electrons are transferred by external soluble mediators between electrodes and biocatalysts. Potential mediators for bio-electrocatalysis include NAD(P)H, flavin adenine dinucleotide (FAD), flavin mononucleotide (FMN), pyrroloquinoline, methyl viologen, anthraquinone-2,6-disulfonate, neutral red (NR), haem and other transition metals.[58,61] MET may result in the principal thermodynamic losses, but will enable large communication distance and cascade reactions.[62]

3.2 Catalysts

In electrocatalysis, catalysts are used to accelerate CO_2 reductions, and increase the specificity towards CO_2 over H^+. Two major types of catalysts used in electrocatalysis are metals and enzymes. Even further, metals can be classified as metals, metal oxides and alloys. Table 1 provides an overview of widely used catalysts.

3.2.1 Metal catalysts. Metal catalysts have been widely applied as CO_2 reduction catalysts. For example, Au, Ag and Zn are typical metal materials that can convert CO_2 into CO. Bi,

Table 1 Overview of catalysts in electrocatalysis

Type	Materials	Main product	Potential	Faradaic efficiency	Ref.
Metal	Au	CO	−0.6 V *vs.* RHE	83%	186
	Au_{25} nanosphere	CO	−0.57 V *vs.* RHE	73.7%	187
	h-Zn	CO	−0.95 V *vs.* RHE	85.4%	188
	Pd NPs	CO	−0.89 V *vs.* RHE	91.2%	109
	Ag nano-corals	CO	−0.6 V *vs.* RHE	95%	189
	β PdHx@Pd	CO	−0.7 V *vs.* RHE	93.4%	190
	β PdHx@Pd	Formic acid	−0.1 V *vs.* RHE	98.9%	190
	Pd	Formic acid	−0.25 V *vs.* RHE	94%	191
	3D tin	Formic acid	−1.2 V *vs.* RHE	90%	192
	Cu foam	Ethylene	−0.8 V *vs.* RHE	55%	70
	Cu	Ethylene	−0.54 V *vs.* RHE	70%	68
	Cu hollow fibers	CO	−0.4 V *vs.* RHE	75%	193
	Ag 3D foam	CO	−0.99 V *vs.* RHE	94.7%	194
	Cu-HNs foam	CO	−0.5 V *vs.* RHE	60%	195
	Zn dendrite	CO	−1.1 V *vs.* RHE	70%	196
	Bi nanotubes	Formic acid	−1.0 V *vs.* RHE	97%	197
	Bi	Formic acid	−0.9 V *vs.* RHE	92%	198
	Polycrystalline Cu	Ethylene	−0.9 V *vs.* RHE	15%	69
	Polycrystalline	Ethanol	−0.9 V *vs.* RHE	7.6%	69
Metal-oxide catalysts	RuO_2/TiO_2 NTs	Methanol	−0.8 V *vs.* SCE	60.5%	199
	RuO_2/TiO_2 NPs	Methanol	−0.8 V *vs.* SCE	40.2%	199
	Au–CeO_x/C	CO	−0.89 V *vs.* RHE	89.1%	200
	Oxide-derived Au	CO	−0.35 V *vs.* RHE	96%	201
	SnO_2/NSC	Formic acid	−1.15 V *vs.* RHE	94.4%	202
	Mo–ZnO	CO	−1.0 V *vs.* RHE	39.8%	203
	Bi/Bi_2O_3	Formic acid	−0.87 V *vs.* RHE	90.4%	204
Alloy catalysts	Pd–Pt NPs	Formic acid	−0.4 V *vs.* RHE	88%	205
	Au–Cu NPs	CO	−0.73 V *vs.* RHE	65%	206
	Pd@Au	CO	−0.5 V *vs.* RHE	80%	207
	PdAg	CO	−0.75 V *vs.* RHE	87.5%	208
	Au-bipy-Cu	Acetaldehyde	−0.9 V *vs.* RHE	25%	209
	Cu–Pt NCs	Methane	−1.6 V *vs.* SCE	21%	210
	Cu–Sn	CO	−0.6 V *vs.* RHE	90%	211
	Tungsten diselenide nanoflakes	CO	−0.164 V *vs.* RHE	24%	212
	Au NPs-coupled ZnTe/ZnO array	CO	−0.7 V *vs.* RHE	97%	213
	CuAg wire	Ethylene	−0.7 V *vs.* RHE	60%	214
	CuAg wire	Ethanol	−0.7 V *vs.* RHE	25%	214
	Cu_4Zn	Ethanol	−1.05 V *vs.* RHE	29.1%	215

NPs, nanoparticles.

Sn, Pb and In with a d^0 electronic configuration that can convert CO_2 into formic acid. Au nanoparticles can transform CO_2 into CO with an 88.6% faradaic efficiency.[63] Ag nanoparticles with Ag(211) and Ag(110) surfaces are favourable in CO formation of CO_2 electroreduction.[64] A Bi monolayer catalyst has been reported to convert CO_2 into formic acid with a 99% faradaic efficiency for over 75 hours.[65] A Sn electrode with a rough surface and large superficial area can reduce CO_2 into formic acid with an 85% faradaic efficiency.[66,67]

As the most distinctive metal material having the potential to convert CO_2 into C_2 and C_3 products, Cu has attracted intense interests. The major C_2 products of the Cu-catalysed CO_2 reductions are ethylene and ethanol.[68,69] Modification of the surface and design of the nanostructure of metal electrodes is significant. Flat surfaces of the bulk metal electrode show limited activity in CO_2 reduction, while electrodes consisting of porosity nanoparticles on the surface showed increased activity. For instance, Cu foam can be used to convert CO_2 into ethylene and ethane with a 55% faradaic efficiency due to the porous surface that helps to expose more active sites during catalysis, while Cu nanoparticles without any modification can only lead to the formation of methane with 57% selectivity.[70] In addition, the crystal facet of a metal electrode can also influence the catalytic performances.[71] Heijne *et al.* tested biocompatible and costless cathode materials including heat-treated stainless steel felt, untreated stainless steel felt and graphite felt, and reported a 60.8% current efficiency and 21.9% energy efficiency using the heat-treated stainless steel felt biocathode.[67]

3.2.2 Metal oxides. The large-scale application of noble metal catalysts in CO_2 reduction has been hindered by their high cost and limited availability, so metal-oxide catalysts have been widely explored as substitutes. Transition metal oxides such as TiO_2 and RuO_2 can convert CO_2 into methanol, SnO_2 and Bi_2O_3 can convert CO_2 into formic acid, and MoO_2 and ZnO can produce CO as the main products in CO_2 reduction.[72,73] Moreover, Cu_2O exhibits remarkable selectivity towards C_{2+} compounds, and the formation of C_3 and even C_4 products have also been reported based on a synergistic effect between Cu_2O and chloride adsorption that results in a high density of Cu^{1+} species.[74] Abundance of Cu^{1+} species enhances CO adsorption and leads to a more stable coverage of various intermediates and prolongs the residence time of intermediates and the

formation of longer carbon chain products.[75] Cheng *et al.* identified three active sites for Cu oxide based CO_2 electroreduction through molecular dynamic simulation, and suggested that planar-square and convex-square sites favour ethylene production and step-square sites favour alcohol generation.[76]

The morphology of electrodes can influence the electrocatalytic performances for the CO_2 reduction. Compared with electrodes with a smooth surface, electrodes with a rougher surface exhibit high density of under-coordinated sites and display enhanced hydrocarbon selectivity.[77] Sargent *et al.* reported a catalytic trend in which sharper structures such as nanoneedles, nanowhiskers and nanodendrites favour C_{2+} production.[78] Sharp tips have been reported to improve bubble nucleation, stabilize cations, and increase local pH to limit the protonation of bound CO, and improve production specificity of multi-carbon products.[79–82] Kim and Palmore designed Cu(I)–halide-derived catalysts that promote adsorption of carbon intermediates and C–C coupling reactions, improve the faradaic efficiency of C_{2+} products to 72.6%.[83] Anwer *et al.* reported the development of a reduced graphene oxide/tungsten oxide modified cathode and the production of acetate with the 86% coulombic efficiency.[84]

3.2.3 Alloys. Alloys have been developed to improve faradaic efficiencies for CO_2 reduction from to their parent metals. Chen and Sargent modified the electronic structure of Cu with boron dopant that can suppress the formation of C_1 species and decrease the energy barrier for the formation of C_2 species, leading to a 79% faradaic efficiency of C_2 products on boron-doped Cu catalysts with a stable and prolonged lifespan of over 40 hours.[85] Christophe *et al.* reported that alloys 10% Au could completely suppress hydrocarbon formation, and improve the selective formation of CO.[86] Ma *et al.* reported that the symmetry of the Pd–Cu multi-components could significantly affect CO_2 reduction selectivity, with ordered Pd–Cu multi-components favouring the production of C_1 compounds, while asymmetric Pd–Cu multi-components exhibit high selectivity towards C_2 compounds.[87,88] Mixed-metal oxides are also used as catalysts to achieve synergetic effects of the parent oxides.[89]

3.3 Integration of electron transfer and catalytical materials

Carbon dioxide electroreduction requires electron transfer as the driving force and catalytical sites to bind with the CO_2 molecules. Hence, good electrocatalysts should integrate electron transfer materials and materials with catalytic activity. Depending on the structures, electron transfer and catalytical materials complexes can be divided into one-dimensional, two-dimensional, or three-dimensional composites (Fig. 3).

3.3.1 One-dimensional composites. Composites characterized by the morphology of nanotubes, nanowires, nanofibers and nanorods are typically regarded as one-dimensional composites. One-dimensional materials have been extensively studied due to their unique tube-like nanostructure, large specific surface area, abundant catalytically active sites, preferentially selected crystal facets and oriented electron and mass transfer.[90] The large surface area of one-dimensional materials helps expose more catalytically active sites for the formation and adsorption of key intermediates in CO_2 electroreduction. The unique tube-like nanostructure of one-dimensional materials can provide a shortened pathway to facilitate the transport of electrons and protons, and thus improves the conversion efficiency of CO_2 into other chemicals. In addition, one-dimensional materials can easily composite with other catalysts to form high-performance composites electrode materials for CO_2 electroreduction.

Major products of one-dimensional composites electrode materials for CO_2 electrocatalysis are usually methane, CO, and formic acid. Several improvements have been attributed to one-dimensional electrode materials for CO_2 reduction, such as heteroatom doping, composite with other high active catalysts, and catalysis on crystal facets. For instance, nitrogen-doped CNTs have better catalytic activity due to the introduction of nitrogen defects that can mediate the electronic structure and regulate the atomic arrangement on the complexes surface. Sun *et al.* reported In-doped SnO_2 hollow nanofibers which can improve the electrocatalytic performance by limiting the grain size of SnO_2 and increasing the electron density of Sn to produce formic acid with a faradaic efficiency of 86.2%.[91] Liang *et al.* fabricated Ag nanowires which can expose a large amount of

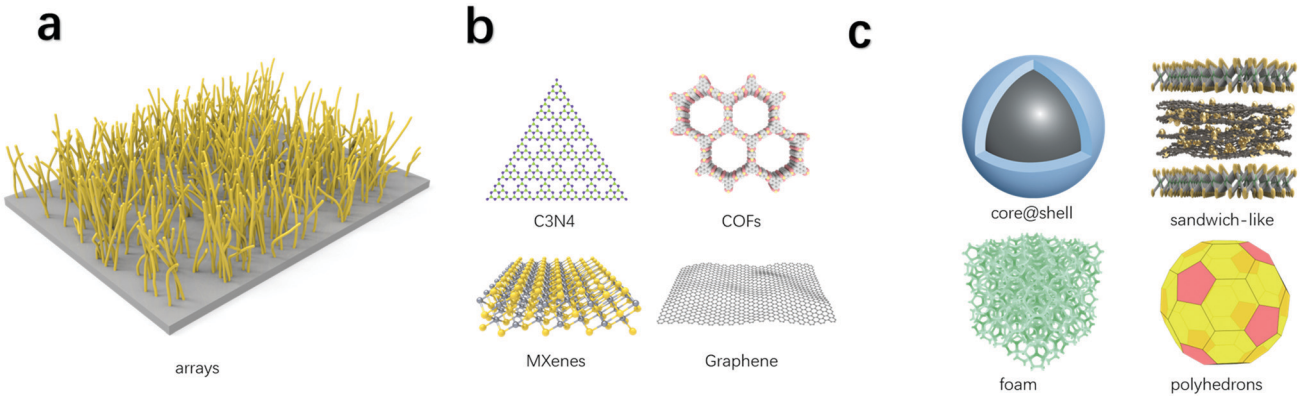

Fig. 3 Electron transfer and catalytical materials complexes. (a) One-dimensional composites. (b) Two-dimensional composites. (c) Three-dimensional composites.

Table 2 Overview of one-dimensional composites

Materials	Main product	Potential	Faradaic efficiency	Ref.
PEI/NGCNT	Formic acid	−1.8 V *vs.* SCE	87%	216
Pd/PANI-CNT	Formic acid	−0.8 V *vs.* SCE	83%	217
NiSA-N-CNT	CO	−0.7 V *vs.* RHE	91.3%	218
Cu/SnO_x-CNT-#7	CO	−0.99 V *vs.* RHE	89%	219
Cu/SnO_x-CNT-#12	Formic acid	−1.09 V *vs.* RHE	79%	219
AuCNT	CO	−0.55 V *vs.* RHE	70%	220
g-C_3N_4/MWCNT	CO	−0.75 V *vs.* RHE	60%	221
NCNTs-ACN-850	CO	−1.05 V *vs.* RHE	80%	222
CN-H-CNTs	CO	−0.5 V *vs.* RHE	88%	223
CoPP@CNT	CO	−0.6 V *vs.* RHE	98.3%	94
NFe-CNT/CNS	CO	−0.59 V *vs.* RHE	69%	224
Ni@NCNTs	CO	−0.8 V *vs.* RHE	99.1%	225
CdS-CNT	CO	−1.2 V *vs.* RHE	92%	226
Ni-CNT-CC	CO	−0.53 V *vs.* RHE	90%	227
MWNT/PyPBI/Au	CO	−1.4 V *vs.* Ag/AgCl	90%	228
CoPc-py-CNT	CO	−0.63 V *vs.* RHE	98%	229

Ag(200) facets that can provide more electroactive sites on the surface of Ag nanowires to facilitate the conversion from CO_2 to CO with a faradaic efficiency of 81%.[92] Wang *et al.* constructed a N/Ni nanoparticles (NPs) @CNT/Graphene hybrid electrode which encapsulated Ni nanoparticles and N dopants in CNTs, which could achieve a high faradaic efficiency of 97.7% to convert CO_2 into CO.[93] Zhu *et al.* developed protoporphyrin IX cobalt (CoPP) @CNT composites that achieve a 98.3% faradaic efficiency for CO products in CO_2 electroreduction.[94] Xu *et al.* reported the production of 80.9 mL L^{-1} methane using the hybrid graphite felt biocathode at −1.4 V *vs.* Ag/AgCl cathode potential.[95] Details of more widely used one-dimensional composites are summarized in Table 2.

3.3.2 Two-dimensional composites. Two-dimensional materials are composed of a single layer or a layer of atoms or molecules. Composites with morphology of membrane, nanosheets and superlattice are usually recognized as two-dimensional materials (Fig. 3b). Due to their planar structure, two-dimensional composites can expose their catalytically active sites more uniformly, and provide high density of surface atoms and edge defects that can exhibit extraordinary electrocatalytic performance in CO_2 reduction.[96] Moreover, the large surface area and shorter diffusion path for charge transfer in two-dimensional materials can also benefit the conversion efficiency of CO_2 electroreduction.

Different from one-dimensional composites that can only lead to the formation of C_1 products, two-dimensional composites have the possibility in forming C_{2+} products such as ethanol and propanol. For example, Rinaldi *et al.* reported a flower-like composite Graphene/ZnO/Cu_2O with the combination of graphene, ZnO nanoparticles and Cu_2O nanoparticles, and produced propanol with a faradaic efficiency of 30%.[97] Cu_2O has the ability to stabilize the adsorption of CO which is a key step for the further formation of C_2 or C_{2+} species, while ZnO is able to stabilize Cu atoms to strengthen Cu–CO^- links, graphene in this composite serves as a highly electronically conductive matrix to support the catalysts, so Graphene/ZnO/Cu_2O took advantage of the synergic effect of these three materials to achieve chain-growth and acquire propanol as the final product. Rezazi *et al.* designed Pt@reduced graphene oxide and achieved the formation of methanol at −0.3 V *vs.* Ag/AgCl with a faradaic efficiency of 41%.[98] The pyridine structure in rNGO can accept a proton to form pyridinium ion which has a synergic effect with Pt to stabilize the adsorption of PyH^+–COOH that can lead to the formation of methanol. Yuan reported Graphene oxide-VB_6-Cu-2 composites that can convert CO_2 into ethanol with a faradaic efficiency of 56.3% over 24 hours.[99] Pyridoxine (VB_6) is an N-containing material that has high catalytical activity to ethanol,[100] while graphene oxide nanosheets can provide a large amount of edge sites such as carboxyl groups to facilitate the CO_2 electroreduction, and Cu nanoparticles in this composite can serve as high performance catalysts to improve the conversion efficiency of ethanol from CO_2. Sekar developed N-doped graphene-Co_3O_4-30 nanohybrid catalyst that can transform CO_2 into formic acid with a faradaic efficiency of 83% at an onset potential of −0.82 V *vs.* SCE.[101] The pyridinic defects in NG-Co_3O_4-30 hybrids are able to convert CO_2 into CO at a low overpotential, and Co_3O_4 has the selectivity to catalyse CO_2 into formic acid. Details of widely used two-dimensional composites are summarized in Table 3.

3.3.3 Three-dimensional composites. The structures of three-dimensional composites can be complex. Three-dimensional composites usually have the advantages of high surface area that can increase the transport efficiency for charge and expose more catalytically active sites for CO_2 adsorption. The design and construct of three-dimensional electrode materials for CO_2 reduction is immensely significant. Based on current state of the art, there are five typical three-dimensional nanostructures: arrays, core–shell, sandwich-like, foam and polyhedrons (Fig. 3c). Details of widely used three-dimensional composites are summarized in Table 4.

Array nanostructures composed of a series of nanowires that are vertically grown on a substrate. Vertical channels in array nanostructures can shorten the diffusion path, accelerate the charge transfer efficiency, and composite with catalyst nanoparticles inside or outside the channels to help improve the overall performances of the electrodes. Cai *et al.* fabricated Cu nanoarrays as the electrode for CO_2 reduction, and the Cu arrays function as rapid pathways for the transport of charge and CO_2 molecules, the high electrocatalytic activity of Cu also provide the selectivity for the formation of ethanol and propanol, so this array-structure electrode can finally achieve a 67% faradaic efficiency of the CO_2 electroreduction.[102]

For core–shell nanostructures, the shell protects the extremely active nanoparticles inside to avoid deactivation during the reduction process, as well as hybridize electronic structure to improve the catalytic performance of the catalyst. In addition, the shell is relatively more active than the core, and the surface modification of the shell is easier to operate than other nanostructures. Polyhedron nanostructures are widely used in metal electrodes because of their specific crystal facets. Sun designed a unique sandwich-like electrocatalyst for CO_2 reduction, the ultrathin tin metal layers that confined in graphene can provide enough space for the diffusion of electrolyte and expose abundant

Table 3 Overview of two-dimensional composites

Materials	Structure	Main product	Potential	Faradaic efficiency	Ref.
HNCM/CNT	Membrane	Formic acid	−0.9 V *vs.* RHE	81%	230
Ni–N-Gr	Nanosheet	CO	−0.7 to −0.9V *vs.* RHE	90%	231
Fe–N-C	Nanosheet	CO	−0.9 V *vs.* NHE	80%	232
p-NG-Cu-7	Nanosheet	Ethylene	−0.9 V *vs.* RHE	19%	233
NG-Co_3O_4-30	Nanosheet	Formic acid	−0.95 V *vs.* SCE	83%	101
Ag_2S/N-S-doped rGO	Nanosheet	CO	−0.76 V *vs.* RHE	87.4%	234
In_2O_3-rGO	Nanobelt	Formic acid	−1.2 V *vs.* RHE	84.6%	235
GO-VB_6-4	Nanosheet	Ethanol	−0.4 V *vs.* RHE	36.4%	100
GO-VB_6-4	Nanosheet	Acetone	−0.4 V *vs.* RHE	8.9%	100
30.87 wt% PO-5 nm Co/SL-NG	Nanosheet	Methanol	−0.9 V *vs.* SCE	71.4%	236
SnO_2/0.14@N-rGO	Nanosheet	Formic acid	−0.8 V *vs.* RHE	78%	237
NapCo@SNG	Nanosheet	CO	−0.8 V *vs.* RHE	97%	238
w-CCG/CoPc-A Hybrid	Nanosheet	CO	−0.79 V *vs.* RHE	91.5%	239
FeN_5	Nanosheet	CO	−0.46 V *vs.* RHE	97%	240
FePGF	Nanosheet	CO	−0.54 V *vs.* RHE	98.7%	241
Ni^{2+}@NG	Nanosheet	CO	−0.68 V *vs.* RHE	92%	242
Pt@rNGO/GCE	Nanosheet	Methanol	−0.3 V, 2.0 V *vs.* Ag/AgCl	41%	98
Phen-Cu/G	Nanosheet	CO	−0.6 V *vs.* RHE	90%	243
Fe/NG-750	Flake-like sheet	CO	−0.57 V *vs.* RHE	80%	244
Ni-N4	Nanosheet	CO	−0.81 V *vs.* RHE	99%	245
AuNP-GNR	Nanoribbon	CO	−0.66 V *vs.* RHE	92%	246

Table 4 Overview of three-dimensional composites

Materials	Structure	Main product	Potential	Faradaic efficiency	Ref.
SnO_2/CC	Hierarchical with SnO_2 nanosheets	Formic acid	−1.6 V *vs.* Ag/AgCl	87%	7
NG-800	Foam	CO	−0.58 V *vs.* RHE	85%	8
FePGH-H	Porous hydrogels	CO	−0.49 V *vs.* RHE	92.1%	247
Cu/C	Octahedron	Ethanol	−0.5 V *vs.* RHE	34.8%	248
Cu/C	Octahedron	Methanol	−0.3 V *vs.* RHE	43.2%	248
NGQDs	Quantum dots	Ethanol	−0.78 V *vs.* RHE	16%	249
NGQDs	Quantum dots	Ethylene	−0.75 V *vs.* RHE	31%	249
GN/Sn	Sandwich-like	Formic acid	−1.8 V *vs.* RHE	89%	103
GN/ZnO/Cu_2O	Flower-like	Propanol	−0.9 V *vs.* Ag/AgCl	30%	97
Co–N_5/HNPCSs	Core@shell	CO	−0.73 V *vs.* RHE	99.2%	250
Fe–N–C	Rhombic dodecahedron	CO	−0.47 V *vs.* RHE	93%	251
NPC-Pt	Copper skeletons and platinum shells	Dimethyl carbonate	−2.24 V *vs.* Ag/AgCl	81%	252

surface atoms as catalytically active sites for CO_2 adsorption.[103] Wang developed Sn–Cu/SnO_x with a core–shell nanostructure for CO_2 reduction to achieve a high faradaic efficiency above 98% with formic acid as the main product, the *in situ* reconstructed Sn/SnO_x interface can facilitate the binding of the HCOO* intermediate during the reduction process and thus result in an extremely high faradaic efficiency.[104] Yakobson *et al.* developed a three-dimensional N-doped graphene foam for CO_2 reduction, this hierarchical foam provides a large interfacial area for the penetration of electrolyte and offers copious catalytically active sites to adsorb CO_2, the maximum faradaic efficiency for CO production of this foam-like catalyst can reach 85% at a lower overpotential (−0.47 V) for at least 5 h.[8]

Three-dimensional composites with arrays, sandwich-like, core–shell and foam nanostructures can improve the catalytic performance with its huge surface area, and thus expose more catalytically active sites during the reactions. In the design of three-dimensional catalysts for CO_2 electrochemical reduction, there is a trend to construct hierarchical structures, including foam, flower-like, sandwich-like, and other three-dimensional structures, to improve surface areas and pore volumes. Large surface areas and pore volumes can provide increased catalytically active sites for CO_2 reduction, decrease contact resistance, facilitate electron transfer and mass transfer, as well as suppress the aggregation of active sites. Ma and Han synthesized a three-dimensional dendritic Cu–Cu_2O composite with minimal contacting resistance between electrocatalysts and substrates, increased exposed active sites and suitable Cu^I/Cu^0 ratios, and managed to convert CO_2 into acetic acid and ethanol at a low potential of −0.4 V *vs.* RHE with 80% faradaic efficiency.[105] Nwanebu *et al.* developed a three-dimensional polyactic acid lattice cathode with Ni/Fe/Mn-based coatings, and exhibited stable production of 50 ml d^{-1} methane and 185 mg d^{-1} acetate at ~100% Coulombic efficiency.[106]

To further improve the catalytic efficiency in electrocatalysis, it is crucial to design and construct new electrode materials. Based on the current state of the art, we propose that the next generation of electrode materials should consist of the composite of catalysts and electron transfer materials with spatial structures. To optimize the catalytic activity and product selectivity, the catalyst of the composite should be filtered from nano sizes and even crystal planes. Different crystal planes of

the same nanoparticle may have very different catalytic properties. In-depth studies evaluating the impact from various crystal planes in catalysis should be performed. As for electron transfer materials, the most significant point is to improve the electron transfer efficiency. The improvement of electron transfer efficiency, design and modification of catalyst materials will become the direction for future development of CO_2 electroreductions.

3.3.4 Size effect, crystalline surface, and interface modification of electro transfer and catalytical materials. In addition to the morphology and structure of electrode materials, size effect, crystalline surface and interfaces modification of electrodes can also play important roles in CO_2 electroreduction.

Size effect has a significant impact on the catalytical activity and products selectivity of electrode materials. For instance, Au nanoparticles with size <5 nm tend to produce H_2, while Au nanoparticles with sizes ~ 8 nm have better selectivity in the formation of CO, these results can be explained as the number of low-coordinated sites increasing on small size nanoparticles and these low-coordinated sites suppress the formation of CO.[63] Nanosized particles such as Bi, Sn, Pb can be well-dispersed in the electrodes, and nano structure can provide larger surface area since the particles have closer contact than catalysts with macro size. Higher surface area usually means the catalysts can expose more active sites for CO_2 to adsorb and then reduce to other chemical products, and hence improve the overall catalytical activity of the electrode materials. Liu *et al.* developed an N-doped PC61BM ([6,6]-phenyl-C_{61}-butyric acid methyl ester) (N-C61) nanostructure electrocatalyst, and reported stable production of formate with 91.2% faradaic efficiency at a moderate overpotential of 700 mV (Fig. 4).[107,108] Their result showed better performance for CO_2 reduction by the nano structure. Sn particles can have closer contact with electrolyte when their size in the nano scale, and this property will be beneficial in improving the efficiency of electron transfer. Gao *et al.* also described the size-dependent catalytic activity of Pd nanoparticles in CO_2 electroreduction, the faradaic efficiency for CO production can be increased from 5.8% to 91.2% with the size of Pd nanoparticles decreasing from 10.3 nm to 3.7 nm.[109] Small size nanoparticles can expose more edge catalytic sites to adsorb key intermediates in CO_2 electroreduction, and size control can change the ratio of edge and terrace sites as well as the electronic structure of nanoparticles to improve the electrocatalytic performances needed for CO_2 reduction.

Tuning the crystal facets can be regarded as another feasible approach to achieve high electrocatalytic activity and products selectivity for CO_2 reduction. Different crystal facets of the same catalysts may lead to the formation of different products. Rosen *et al.* found that Ag electrodes with Ag(211) facets have stronger adsorption of COOH intermediates which can improve CO production rates and selectivity in CO_2 electroreduction.[64] Zhang *et al.* adjusted the Cu-based catalysts with abundant Cu(100) facets which can lead to the formation of C_{2+} products with 40.5% conversion efficiency in CO_2 electroreduction.[110] It has been proven that Cu(100) facets can lower the dimerization energy barrier,[111] provide strong stabilization for CO intermediates on the surface of catalysts, and thus lead to the growth of carbon chain. Wang *et al.* found that Cu(110) facets in Cu nanocubes can have better selectivity for C_2 and C_{2+} products in CO_2 electroreduction, while Cu(111) facets only have little electrocatalytic activity.[112] Kim *et al.* reported that the Zn(101) facet is more favourable in producing CO in CO_2 electroreduction, while the Zn(002) facet tends to produce H_2.[113] According to DFT calculated ions, Zn(101) facet has better ability to stabilize COOH intermediates due to its lower reduction potential from CO_2 to CO, and this feature can improve the electrocatalytic performance of the electrode material.

Interfaces modification has gained increasing attention since most of the CO_2 electrocatalysis have involved reactions at the liquid–solid–gas three phases. As a result, the modification of interfaces can optimize the electrocatalytic performance of the electrode materials. CO_2 electrocatalysis usually occurs in the presence of aqueous electrolytes, and hydrogen evolution reaction will compete with the formation of products due to their low overpotential. To achieve better interface control in electrocatalysis, surface modification has been applied in some of the electrode materials. For instance, Li *et al.* covered a thin layer of nitrogen-doped carbon on the Cu surface, this thin carbon layer can provide abundant active sites due to the nitrogen defects, and function as a protective shell to resist the morphological change of the catalytical active Cu to achieve a high faradaic efficiency of 90% from CO_2 to C_2 products.[114] Cai *et al.* modified the Cu nanoarray electrode with polytetrafluoroethylene (PTFE) on the surface to achieve a 67% faradaic efficiency for ethanol and propanol products in CO_2 electroreduction, the PTFE here can change the electrode surface from aerophobic to aerophilic state which improves the electrocatalytic performance for the electrode.[102] Fig. 5 shows that carbon nanotube (CNT) was modified with epichlorohydrin dimethylamine copolymer (EDC) and the performance of electrocatalysis was improved.[108]

We propose that next-generation electrode materials for bio-electrocatalysis should combine the nanostructure design,

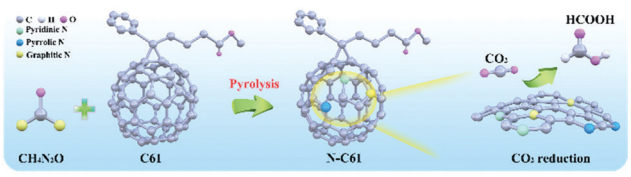

Fig. 4 N-C61 electrocatalysts exhibit efficient formate production. (a) The synthesis procedure for N-C61 nanostructure electrocatalyst. (b) Comparison of maximum faradaic efficiency of N-C61 for formate production with other metal electrocatalysts.

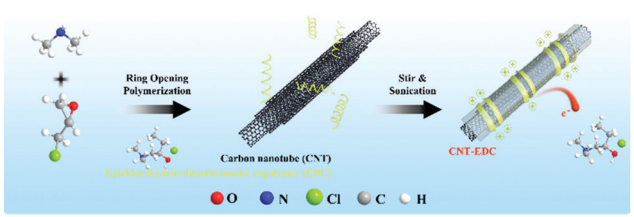

Fig. 5 EDC-modified CNTs as metal-free carbonaceous electrocatalysts.

control of size effect, selectivity in crystal facets and modification of interfaces to improve the electrocatalytic performance. To optimize the catalytic activity and product selectivity, the electrode materials should be filtered from nano sizes and crystal facets to achieve high conversion efficiency for value-added products. In-depth studies of impacts from various crystal planes in catalysis should be performed. Modification of interfaces should focus on the adjustment of hydrophobic/hydrophilic or aerophobic/aerophilic properties of the electrode surface to optimize the performance.

3.4 Electrolysers

In bio-electrocatalysis, the electrolyser is a system using electricity for reduction-oxidation reactions, typically including CO_2 reduction reactions and oxygen evolution reactions, and determines the local environment around the electrode. Common configurations of electrolysers include H-cell, flow-cell and membrane electrode assembly cell (MEA-cell) electrolysers.[115] The H-cell electrolyser has been widely applied because of its robust and simple operation over a wide range of catalysts and electrodes. However, carbon dioxide first has to be dissolved into the electrolyte and then to the cathode to be reduced. Further, the poor CO_2 mass transport rate limits current density, and restricts its commercial applications.[116] The flow-cell electrolyser and MEA-cell electrolyser both utilize gas diffusion electrodes and a continuous flow of electrolyte through the electrolyser, with improved mass transport and current densities, as well as the opportunity of online adjustment of operating procedures.[117] However, flow-cell electrolysers may exhibit potential risk of crossover of cathodic and anodic products, and poor stability in alkaline electrolytes, which reduces the overall productivity and energy efficiency.[118] The MEA-cell electrolyser, on the other hand, assembles the catalytic layer of cathodic gas diffusion electrode closely with the bipolar membrane without catholyte, and reduces ohmic losses and catalyst contamination, while increasing overall energy efficiency and stability.[119] Thus, MEA-cell electrolysers have attracted increased attentions, especially for C_{2+} products and commercialization purposes. Li *et al.* coated the Cu catalyst with *N*-aryl-substituted tertrahydro-4,4′-bipyridine organic films, and managed to produce ethylene with a 64% faradaic efficiency and a 20% energy efficiency at the 80 mA cm^{-2} current density for 190 h.[120] Endorödi *et al.* developed a multilayer electrolyser for CO production, with serial connections of MEA units to increase the electrochemically active surface area, and achieved a 40% CO_2 conversion efficiency, a 95% faradaic efficiency and >250 mA cm^{-2} current densities.[121] Details of MEA-cell representatives are provided in Table 5.

Further improvement of MEA-cell electrolysers includes continuous upgrading of gas diffusion electrodes to sustain high ion mobility while buffering the local environment, improving membrane ion mobilities and robustness to increase process stability and avoid product crossover, increases interface densities of carbon dioxide/catalyst/electrolyte to improve mass transfer efficiency and production rate.[118,122]

3.5 Enzymatic electrocatalysis

In classic electrocatalysis, metal catalysts may exhibit low availability, low selectivity, and high overpotentials. Enzymatic electrocatalysis integrates electrodes for electrons and fast cofactor regeneration with oxidoreductase enzymes or isolated organelles for high selectivity and self-regeneration, and is a valuable addition and even promising alternatives for noble metal catalysts.[123] Both metalloenzymes and non-metalloenzymes can be utilized in enzymatic electrocatalysis and produce a range of products including CO by CO dehydrogenases, formate by formate dehydrogenases, methane and methanol by formate dehydrogenase and formaldehyde dehydrogenase (Fig. 6).[29,32] For example, Reisner *et al.* utilized formate dehydrogenase and metal oxidase TiO_2, and established selective and reversible conversion of CO_2 to formate with a turnover frequency of 11 s^{-1}.[124] Recently, nitrogenases have drawn increasing interest as it has been shown to also reduce CO_2 to produce CO, formate, ethylene, and propene.[32]

Key factors regarding enzymatic electrocatalysis include the activity and stability of enzymes through electrosynthesis environments, the electron transfer efficiency between electrodes and enzymes, as well as the distance between electron donors and enzyme's redox cofactors.[125] Electron mediators and

Table 5 Overview of representative MEA-cell electrolysers

Catalyst	Anolyte	Main product	Cell voltage	Faradaic efficiency	Current density	Stability	Ref.
GDE-PTFE|GDE-PTFE	DI water	CO	−3.6 V	4.3%	755 mA cm^{-2}	—	253
GDE-Ag/Ir nanoparticles|Ti	—	CO	−3 V	95%	>250 mA cm^{-2}	—	254
Cobalt phthalocyanine|Ni	1 M KOH	CO	−2.2 V	>90%	50 mA cm^{-2}	8 h	255
Ni-NCB|IrO_2	0.1 M $KHCO_3$	CO	−2.8 V	>90%	~8 A	6 h	256
Ni–N/C|IrO_2	0.1 M $KHCO_3$	CO	−3 V	>93%	113.6 mA cm^{-2}	—	257
GDE-Ag|IrO_2/C	0.1 M $KHCO_3$	CO	−3.3 V	>90%	200 mA cm^{-2}	—	258
Bi0.1Sn/PTFE|IrO_x/Ti	0.1 M $KHCO_3$	Formic acid	−4.4 V	90%	60 mA cm^{-2}	100 h	259
2D-Bi|IrO_2–C	DI water	Formic acid	−3 V	80%	30 mA cm^{-2}	100 h	260
GDE-CuPc	0.05 M $KHCO_3$	Methane	−4.4 V	62%	190 mA cm^{-2}	110 h	261
FeTPP [Cl]/Cu|IrO_x/Ti	0.1 M $KHCO_3$	Ethanol	−3.7 V	41%	124 mA cm^{-2}	12 h	262
N–C/Cu|IrO_x/Ti	0.2 M $KHCO_3$		−3.67 V	52%	156 mA cm^{-2}	15 h	263
Molecule/Cu/PTFE|IrO_x/Ti	0.1 M $KHCO_3$	Ethylene	−3.65 V	64%	600 mA	190 h	264
Cu|IrO_2 on Ti mesh	0.1 M $KHCO_3$	Ethylene	−3.75 V	40%	120 mA cm^{-2}	100 h	119
CTPI|Ti	0.1 M $KHCO_3$	Ethylene	−3.9 V	66%	208 mA cm^{-2}	100 h	265
Cu-PTFE|IrO_2	0.1 M $KHCO_3$	Ethylene	−4.1 V	65%	215 mA cm^{-2}	50 h	266
Ti-Based bipolar plate|IrO_x/Ti mesh	0.1 M $KHCO_3$	Ethanol/ethylene	−2.41 V	85.6%	12 A	4.5 h	110

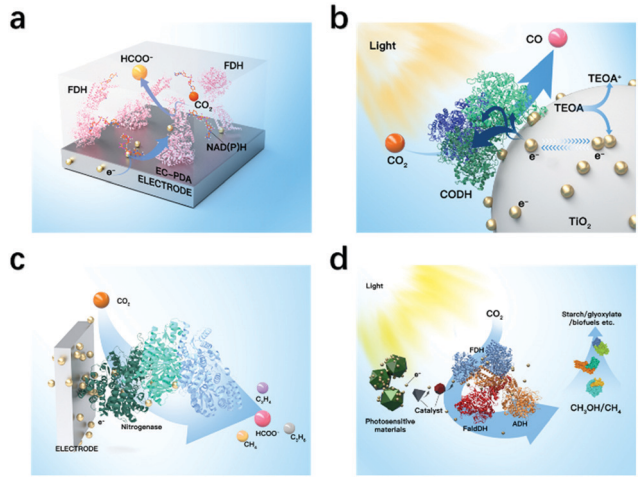

Fig. 6 Representative enzymes used in enzymatic electrocatalysis for fixation. (a) Formate dehydrogenase that converts CO_2 to formate. (b) CO dehydrogenase that converts CO_2 to CO. (c) Nitrogenases. (d) Enzyme cascade of formate dehydrogenase and formaldehyde dehydrogenase that converts CO_2 to methane and methanol.

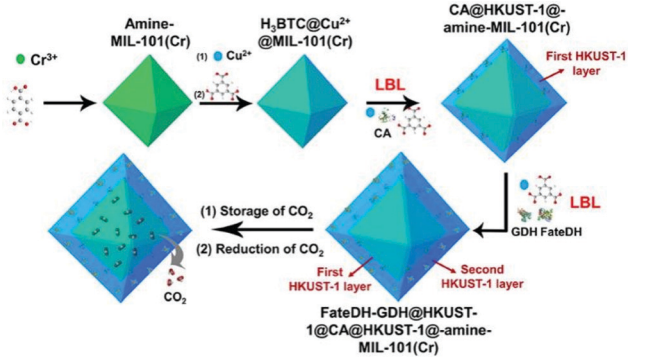

Fig. 7 Schematic illustration of the preparation of HKUST-1@amine-MIL-101(Cr)-based multienzymes for the reduction of adsorbed CO_2. Reproduced with permission from ref. 129, copyright 2019 to Frontiers Media S.A.

heterogeneous materials can be applied to ensure long distance electron transfers or to achieve cascade reactions. Mediators must be carefully selected and sometimes co-immobilized based on the reduction potentials required for the target reaction. Ideally the potential difference between the electron mediator and the enzymatic cofactor should be 50–170 mV.[126] For cascade reactions, uncontrolled intermediates concentrations and distributions may cause mismatched enzymatic kinetics and product inhibition.[127] A co-immobilization of cascade enzymes and their mediators sequentially with precise control of the enzyme ratio and inter-enzyme distance, also called electrostatic substrate channelling, have been employed. Zhang *et al.* encapsulated formate dehydrogenase, formaldehyde dehydrogenase, the organometallic mediator [Cp*Rh(bpy)Cl]Cl and photosensitizer using poly(allylamine hydrochloride)-doped nanofibers, and produced methanol with 90% yield from CO_2.[128] Lv utilized Amine-functionalized MIL-101(Cr) and two-HKUST-1-layer MOFs for CO_2 storage and immobilization of carbonic anhydrase (CA), formate dehydrogenase and glutamate dehydrogenase, and exhibited high catalytic efficiency with the formate yield of 179% (Fig. 7).[129]

While enzymatic electrocatalysis advances with high reaction specificity, robust to co-solvents, and simple workflows, it is limited by the need for enzyme purification, degradation, and regeneration.[32] In addition, many efficient CO_2 reducing enzymes are oxygen sensitive, *e.g.* CO dehydrogenases from *Methanosarcina bakerii*, *Moorella thermoacetica*, and *Carboxythermus hydrogenoformas*, as well as Mo and W-containing formate dehydrogenases, and may require substantial enzyme and process engineering for application.[127,130]

3.6 Bio-catalysis strains and pathways

Several microbes have been described that are able to tolerate low voltage of electricity, and may also conduct electricity and utilize the electrons as the energy source. Thus, microbial electrocatalysis has been developed for CO_2 utilization. Microbial electrocatalysis has many advantages, including self-regeneration, good stability, and the ability to produce a wide range of products. However, compared with enzymatic electrocatalysis it requires a continuous supply of nutrients to keep the microbes functional, and because of its complex metabolic networks, microbial electrocatalysis may have less specificity and efficiency.[57] In microbial electrocatalysis, the identification of suitable host strains and carbon utilization pathways are important. Suitable host strains for bio-electrocatalysis should have robustness and the ability to perform efficient electron transfer, an appropriate metabolic environment for productions of desired products, and more importantly, the compatibility with current reported C_1 utilization pathways. Holtmann *et al.* compared different methanogens, including *Methanococcus vannielii*, *Methanococcus maripaludis*, *Methanolacinia petrolearia*, *Methanobacterium congolense*, and *Methanoculleus submarinus*, and demonstrated that *M. maripaludis* represents a promising methane electrocatalysis producer capable of producing methane with an 8.81 mmol m^{-2} d^{-1} productivity and a 58.9% coulombic efficiency.[131] Host strains that are widely used in CO_2-based bio-electrocatalysis include methanogens, acetogens, *Synechocystis* species, *Clostridia* species, *Microcystis aeruginosa*, and *Acidithiobacillus ferrooxidans*.[57,123]

Current C_1 utilization pathways include the reductive glycine pathway,[9] the Wood-Ljungdahl pathway,[132] the Calvin-Benson-Bassham cycle (CBB cycle),[133] the dicarboxylate/4-hydroxybutyrate (DC/HB) cycle,[134] the reductive TCA cycle,[135] the 3-hydroxypropionate/4-hydroxybutyrate (HP/HB) cycle,[136] the 3-hydroxypropionate (3-HP) bicycle,[137] the crotonyl–coenzyme A (CoA)/ethylmalonyl-CoA/hydroxybutyryl-CoA (CETCH) cycle,[138] the reductive glyoxylate and pyruvate synthesis-malyl-CoA-glycerate (rGPS-MCG) cycle,[139] the PYC-OAH-ACS-PFOR (POAP) cycle,[140] the half-Wood-Ljungdahl-formolase (HWLS) pathway,[141] the ribulose monophosphate (RuMP) Cycle,[142] the xylulose monophosphate (XuMP) cycle,[143] and the serine cycle (Fig. 8).[144] Among these pathways, the CBB cycle, the Wood-Ljungdahl pathway and the reductive glycine pathway attracted

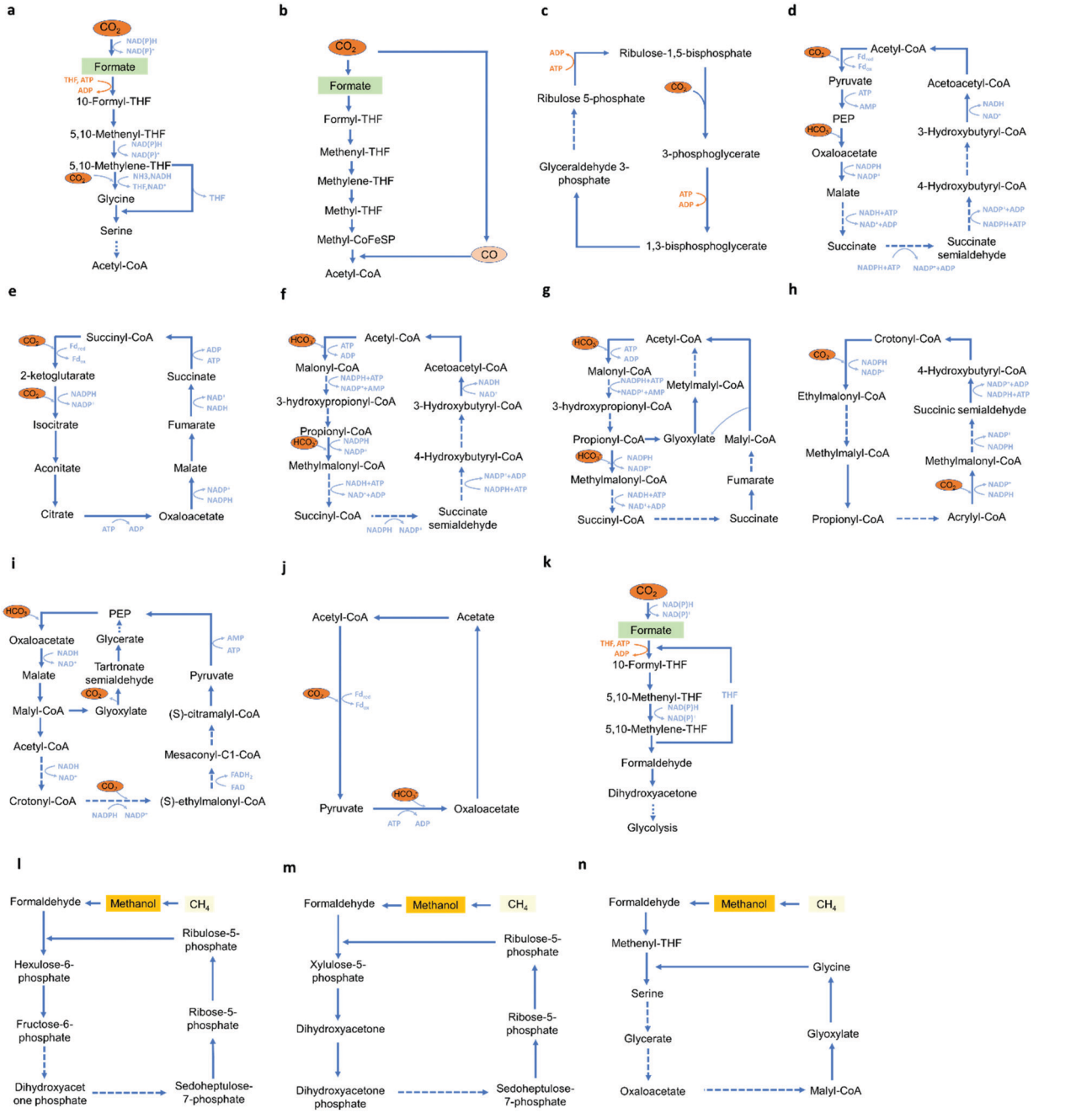

Fig. 8 Representations of current C1 utilization pathways. (a) The reductive glycine pathway. (b) The Wood-Ljungdahl pathway. (c) The CBB cycle. (d) The DC/HB cycle. (e) The reductive TCA cycle. (f) The HP/HB cycle. (g) 3-HP bicycle. (h) The CETCH cycle. (i) The rGPS–MCG cycle. (j) The POAP cycle. (k) The HWLS pathway. (l) The RuMP cycle. (m) The XuMP cycle. (n) The serine cycle.

increased attentions for CO_2 bio-electrocatalysis. The CBB cycle is widely used by plants, algae, cyanobacteria and proteobacteria,[145] and converts CO_2 into glyceraldehyde 3-phosphate using NADPH as the electron donor.[146] Milo *et al.* introduced the complete CBB cycle in *Escherichia coli* and enabled cell growth solely from CO_2 and formate.[147] The Wood-Ljungdahl pathway can be found in euryarchaeota, proteobacteria, planctomycetes and spirochaetes,[145] and can convert CO_2 and a variety of C_1 and C_2 compounds into acetyl-CoA. Within microorganisms utilizing the Wood-Ljungdahl pathway, *Methylorubrum extorquens*, *Cupriavidus necator* and *Clostridium* species have attracted increased attention and are able to produce a wide range of products, including butanol, 2-oxobutyrate and 3-butanediol.[30,36] The reductive glycine pathway is found in *Candidatus* Phosphitivorax anaerolimi, and can convert CO_2 and formic acid into pyruvate.[9] Lee *et al.* reported the introduction of the reductive glycine pathway in *E. coli* and recovered cell growth solely from CO_2 and formate.[148]

4. Integration of electrocatalysis and bio-catalysis

The integration of classic electrocatalysis and bio-catalysis will enable production of a wide range of chemicals from CO_2. The chemically inert nature of CO_2 severely limited its reduction to C_1 compounds, especially through bio-catalysis that requires mild operational conditions. Electrocatalysis has the advantages of high electron transfer efficiency that can accelerate bio-catalysis processes with sufficient and rapid electron supply. Meanwhile, bio-catalysis can solve the side-product problem of electrocatalysis with higher specificity, longer stability, and longer chain length.

A number of C_{2+} products, such as isopropanol,[11] butyric acid,[149] and even C_{6+} products, such as α-humulene,[150] L-erythrulose[151] and terpenes,[152] have been produced (Fig. 9). For example, Chen *et al.* reported the development of the Cu–Ag tandem catalyst, and improved the production of ethylene, ethanol and acetate by 3–6 fold compared with the Cu catalyst.[153] Song *et al.* employed formate dehydrogenase, NADH and NR, to produce formate, and together with *Ralstonia eutropha* was able to produce 485 mg L^{-1} poly(3-hydroxybutyrate) from CO_2.[10] Wu *et al.* reported the production of 1.73 mg L^{-1} lycopene from the flue gas of coal-fired power plant through the direct-electron-transfer strategies, using H_2 as the electron carrier.[154] Bolognesi *et al.* integrated a bio-electrochemical system converting CO_2 to acetate and *Auxenochlor CO2ella protothecoides* converting acetate to the diesel compatible algae oil.[155] More applications of bio-electrocatalysis in production of fuels and chemicals are shown in Table 6. With the rapid development of electrocatalysis, material science and synthetic biology, we foresee in the near future, that bio-electrocatalysis will manage to produce custom-designed, energy-rich products with even longer chain length, such as polymers, and fatty acid derived products.

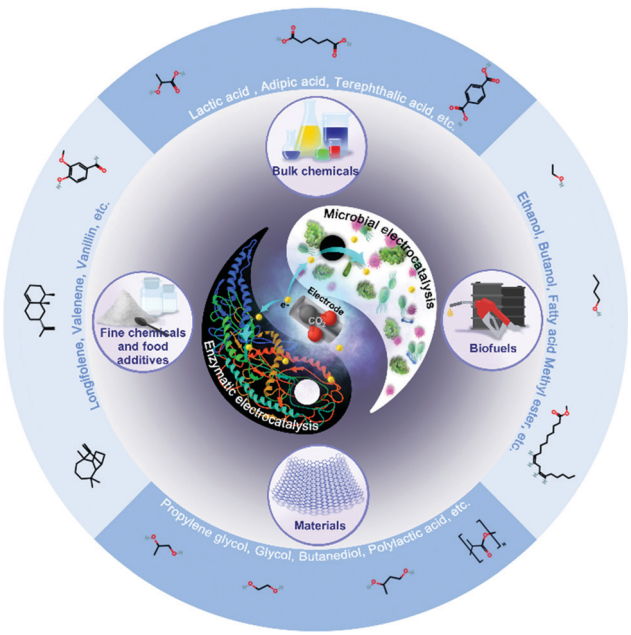

Fig. 9 Applications of bio-electrocatalysis for CO_2 utilizations.

5. Future research directions

5.1 Improving the compatibility between electrodes and biocatalysts

Bio-catalysis can be highly active under mild conditions. Although this requirement can be sustainable and cost-effective, it also restricts the operational conditions of bio-electrocatalysis. Enzymes with their active sites exposed, such as ferredoxin, peroxidase, and cytochrome *C*, are suitable for direct electron transfer.[156] However, it is relatively difficult to keep enzymes close to the electrode while maintaining their stability and activity. Mediators can be used to improve electron transfer efficiencies; however, they also have limitations such as their potential toxicity to biocatalysts, especially enzymes. The utilization of redox polymers and biofilms to co-assemble biocatalysts and electron mediators can enhance the communication between biocatalysts and electrodes on the nanometre and micrometre scale, while improving the biocompatibility, conductivity, and mass transfer rate. For example, Milton *et al.* reported the synthesis of the cobaltocene-functionalized poly(allylamine) to immobilize formate dehydrogenase while mediating electron transfers from the electrode, and produce formate with a 99% faradaic efficiency.[157]

Furthermore, microbial communities have also been described that can improve the electric tolerance and bio-electrocatalysis production. Hogan reported the methanogenesis rate at 0.72 mg methane L^{-1} day^{-1} using the microbial community, and demonstrated that the abundance of *Euyarcheota* and the *Desulfovibrionaceae* phylotype positively corelated with methane production.[158] They also demonstrated that for some species in the community that do not produce methane themselves they may help improve the electron transfer and the overall synthesis.[158]

Optimization of the electrode composition and the electrolyte can also increase the compatibility of electrocatalysis and bio-catalysis.[57,123] For example, Nocera *et al.* developed a Reactive oxygen species-resistant Co–P cathode and substantially reduced the release of toxic metals during aerobic electrocatalysis.[159,160] Liao *et al.* applied a porous ceramic cup to shield the anode to allow efficient diffusion of chemicals while reducing exposure of the cell to toxic reactive oxygen and nitrogen compounds, and produced 140 mg L^{-1} biofuels.[161] Cornejo *et al.* utilized an ultrathin silica membrane to separate abiotic and biotic components while maintaining their electrochemical intereactions.[162] Hass *et al.* developed a gas diffusion cathode allowing a direct interaction with gaseous CO_2, and substantially increased the mass transferring rate of CO_2 in salt-based electrolytes.[163] Rodrigues *et al.* utilized a biocompatible perfluorocarbon nano-emulsion as the H_2 carrier and increased acetate production by 190% to the highest reported productivity (1.1 mM h^{-1}).[164] Photoelectrodes, which directly harvest solar energy to provide electrons, have also been developed

Table 6 Key applications of bio-electrocatalysis

Carbon source	Production method	Chain length of products	Production host	Product	Production level[a]	Catalyst	Ref.
CO_2	Microbial transformation	C_1–C_6	*Methanosarcina barkeri*	Methane	15.71 mM d^{-1}	—	183
			C. autoethanogenum	Acetate	2.42 mM L^{-1} d^{-1}	Cds	267
			Acetogen co-culture	Acetate	23.50 mg d^{-1}	—	268
			Sporomusa ovata	Acetate	6.66 mM d^{-1}	—	269
			M. thermoacetica	Acetate	Milligram level per h	Cds	270
			M. thermoacetica	Acetate	Milligram level per h	AuNCs	5
			C. scatologenes	Ethanol	2.14 mg L^{-1} d^{-1}	rGO/biofilm	271
			Synechococcus elongatus	1,3-Propanediol	21 mg L^{-1} d^{-1}	—	272
			Synechocystis sp.	3-Hydroxybutyrate	25.4 mg L^{-1} d^{-1}	—	273
			C. eticum	2-Oxobutyrate	2 mg L^{-1} d^{-1}	—	274
			Clostridium co-culture	Butyrate	1.82 mMC d^{-1}	Carbon cloth	149
			C. necator	Isobutanol	~8.5 mg L^{-1} h^{-1}	Indium foil	275
				3-Methyl-1-butanol	~5.7 mg L^{-1} h^{-1}		
			Microbiome	Acid alcohol mixture	Milligram level per d	Graphite granules	276
			Microbiome	Alcohols	0.34 kg m^{-3} day^{-1}	VITO-Core® GDE	277
		C_{6+}	*C. necator*	α-Humulene	36 mg L^{-1} d^{-1}	Patinum late	150
			Synechocystis sp.	Hydrocarbon fuel	11.12 mg L^{-1} d^{-1}	—	278
	Enzymatic synthesis	C_1–C_6	FDH	Formic acid	0.92 μM h^{-1}	Graphene-based photocatalyst	279
			CA, FDH	Formic acid	48.6 μM h^{-1}	g-C_3N_4/ZIF-8	280
			FDH	Formic acid	225.81 mg L^{-1} h^{-1}	Plain graphite rod	281
			FDH, FaldDH and alcohol dehydrogenase (ADH)	Methanol	0.4 mM h^{-1}	UF membranes	282
			Glyoxylate carboligase	Ethylene glycol	3.5 mM h^{-1}	—	283
		C_{6+}	Multienzyme cascade	Terpenes	0.2 mg L^{-1} h^{-1}	—	152
C1 utilization	Microbial transformation	C_1–C_6	*Methylomonas sp*	Succinate	1.54 mg L^{-1} h^{-1}	—	34
			C. carboxidivorans	Alcohols	Milligram level per d	—	284
			Clostridia	2,3-Butnanediol	0.25 mM d^{-1}	—	285
			M. extorquens	Itaconic acid	2.63 mg L^{-1} d^{-1}	—	286
		C_{6+}	*M. extorquens*	α-Humulene	15.87 mg L^{-1} h^{-1}	—	35
			M. extorquens	Mevalonate	6.6 mg L^{-1} h^{-1}	—	287
	Enzymatic synthesis	C_1–C_6	Multienzyme cascade	Glyoxylate	26.7 mg L^{-1} h^{-1}	—	288
			Multienzyme cascade	L-Erythrulose	126 g L^{-1} h^{-1}	—	151
		C_{6+}	Multienzyme cascade	Starch	17.2 nmol C min^{-1} mg^{-1}	ZnO-ZrO_2	289

Note. [a] Here, we calculate the average value according to the final output in the respective literature. If there is no specific value, it cannot be calculated because it is not given in the article.

for CO_2 fixation and conversion. Current reports integrated photo-electrocatalysis with bio-catalysis mostly used NAD(P)H as the electron mediator and carrier.[165] For example, Guo *et al.* reported the integration of yeast cell factories with indium phosphide based light-harvesting nanoparticles using a polyphenol-based assembly method, and enabled carbon-and energy-efficient production of shikimic acid.[166] Similarly, Hu *et al.* incorporated CdS nanoparticles and a synthetic half-Wood–Ljungdahl-formolase CO_2 fixation pathway in *E. coli*, and improved the anaerobic production of L-malate and butyrate approaching to the theoretical yields.[141]

Future research directions include improvement on the electrochemical surface area, absorption of bio-electrocatalysts, intrinsic conductivity, electron transfer rates, the operational performance and stability, as well as metabolic engineering of microbes to better tolerate electrocatalysis conditions, such as pH, temperature, electrolyte composition and toxic byproducts.[166,167]

5.2 Optimizing the electron transfer efficiency

The electron transfer rate and multi-electron transfer efficiency in bio-electrocatalysis need to be optimized.[168] For enzymatic electrocatalysis, oxidoreductases generally hide active sites in the centre and strictly regulate intra-enzyme electron transfers, that reduces electron transfer efficiency between electrodes and enzymes.[169] By surveying existing electron transfer mechanisms, Dutton *et al.* reported that electrons can travel up to 14 Å within the protein medium without significantly reducing the transfer rate and efficiency.[170] Enzyme engineering has been utilized to improve the communications between electrode and oxidoreductases, including protein truncation to delete unessential peptides and expose active sites, surface modifications (*e.g.* de-glycosylation) to downsize the dimensions of the protein and facilitate electron transfer, and modification of active sites to improve electron channeling.[171] The addition of the redox polymer and the docking motif to immobilize oxidoreductases to the electrode surface and even in the optimal orientation may reduce the distance while improving localized enzyme concentrations, however, the requirement of an monolayer of enzymes may restrict the overall catalyst loading.[167]

In microbial electrocatalysis, most cell membranes are non-conductive.[172] Moreover, microbial pathways can be complicated

in a microbial system since it requires several cofactors to transfer electrons as the driving force. Strategies to efficiently bridge electronic devices and microbial cell factories include direct electron transfer though cytochromes and conductive nanowires, and indirect electron transfer through redox mediators or energy carriers. Currently used protein nanowires include curli fibers,[173,174] pilin-based nanowires,[175] cytochrome wires,[176,177] and conductive fibres of cable bacteria.[178,179] Clarke *et al.* reported the atomic structure of the electron conducting MtrAB protein complex spanning outer membranes of *Shewanella* species, that could connect cells with extracellular electrodes and conduct electrons.[180] Malvankar *et al.* also described the production of cytochrome OmcZ nanowires with high conductivity and stiffness from electric stimulated *Geobacter sulfurreducens* biofilms.[177] Similarly, when analysing the structure of widely spread coronavirus, we identified a number of protein receptors similar to antenna on its surface that accelerate the electron transfer and information exchange of the virus. Future research direction may indicate whether the incorporation of these protein nanowires on the cell surface of microbial cell factories may act as quick and efficient electron transfer channels. One could also build artificial channels that possess effective metabolic pathways to produce high value-added products that enable direct electron harvest for biosynthesis (Fig. 10). Hereby the dependence on cofactors and overall energy consumption could be greatly reduced.

Common mediators and electron carriers of in-direct electron transfer processes include native mediators such as flavins and quinine, electron carriers such as cofactors, H_2 and formate, natural and artificial substances such as humic acid and neutral red, as well as enzyme like hydrogenases and formate hydrogenases.[181] It has been suggested that optimizing the bound flavin cofactor mechanisms could substantially increase the cross-membrane electron transfer.[182] Moreover, Nichols introduced the Pt and Ni based Hydrogen evolution reaction electrocatalysts into *Methanosarcina barkeri*, and achieved conversion of CO_2 to methane with over 81% faradaic efficiency.[183] Liu integrated Mn based H_2 catalysis into *C. necator*, and achieved efficient production of cell mass, fusel alcohols and PHB.[159] Li *et al.* discovered three gene modules and five key genes regarding the NAD^+ generation in *Shewanella oneidensis*, and increased the intracellular NAD(H) concentration by 2.1-fold.[184] Similarly, Yang *et al.* integrated the flavin-generation pathway from *Bacillus subtilis* to *S. oneidensis*, and increased the inward power density by 15.5 fold.[185]

Future research directions include the optimization of the uptake rates of electron donors and electron carriers, as well as the intracellular transportation of electrons, the oxidation of electron donors to release electrons, the reduction of the use of costly catalysts, the development of synthetic biology and metabolic engineering tools of less-characterized electroactive enzymes and microbes, deepening the understanding of cross-membrane and intracellular electron transport mechanisms, and harmonizing heterologous pathways and endogenous metabolisms.[123,181]

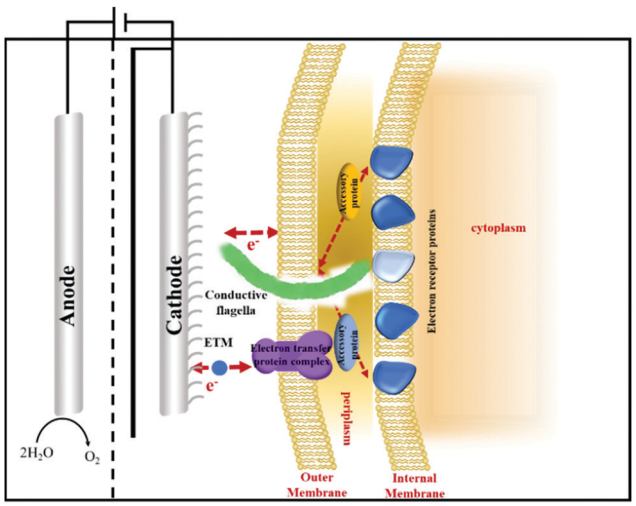

Fig. 10 Illustration of the artificial cell with antenna electron transfer channels on its surface.

6. Outlook

The growing concerns about elevated GHGs emissions calls for immediate shift of fossil fuel dependent industries. Simple capture of CO_2 is no longer enough to hold back the negative effect of greenhouse gases. As a result, transformation of CO_2 into fuels and chemicals has attracted increased attention. Bio-electrocatalysis for CO_2 utilization offers solutions to this challenge through the following aspects. (i) Use of electricity from renewable sources, including solar, wind, tidal, thermal, and hydro. In combination with bio-electrocatalysis, carbon neutral (or in some cases even carbon negative) production of valuable products can be acquired. (ii) Compared with classic electrocatalysis, bio-electrocatalysis has a lower environmental impact, higher selectivity, longer stability, more flexibility for custom-designed products, and a wider product range, especially for products with higher chain length, such as biofuels and biopolymers. (iii) Bio-electrocatalysis showed the superiorities than the bio-catalysis in the two critical steps, including the CO_2 fixation efficiency and the energy utilization efficiency, and bio-electrocatalysis could exhibit greater potentials for producing energy-dense compounds, such as jet fuels.

Future research directions include the characterisation and re-construction of biologically produced electron transferring nanowires and extracellular respiratory modules to improve the energy conversion efficiency and specific productivity. In addition, the identification of more efficient fixation pathways, in terms of conversion rates for the identification of appropriate microbial cell factories having efficient carbon fixation rates, high growth rates, and electron tolerance and utilization efficiency. Other advances could involve the use of complex materials and advanced devices. Two limiting factors of electrocatalysis include the electrons transfer rate and the CO_2 mass transport rate. Bio-electrocatalysis aims to enhance the electron transfer efficiency and the CO_2 utilization rates through the optimisation

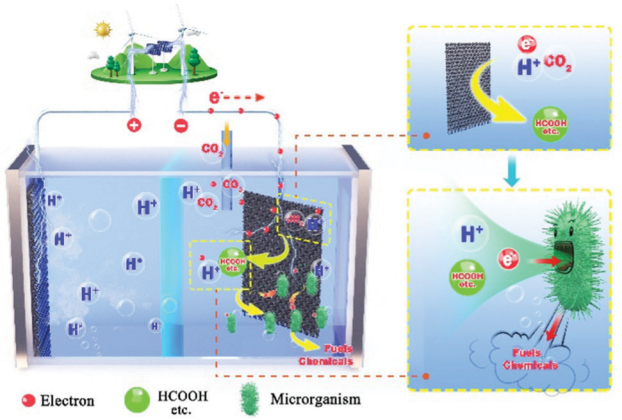

Fig. 11 Illustration of bio-electrocatalysis enabled bio-economy.

of three-dimensional electrode materials and their hybrids, *e.g.*, arrays, core@shell, sandwich-like, foam and polyhedrons. Meanwhile, the continuous development of MEA-cell electrolysers will further enhance bio-electrocatalysis towards commercialisation.

In conclusion, with the advancement of the technologies presented in this review, we expect that bio-electrocatalysis will be able to play a significant role in the future energy and chemical sector (Fig. 11).

Author contributions

X. T. drafted the outline. X. T. and J. N. wrote the manuscript. J. N. supervised the research. All the authors have read and approved the final manuscript.

Conflicts of interest

The authors declare no competing interests.

Notes and references

1 Z. Liu, K. Wang, Y. Chen, T. Tan and J. Nielsen, *Nat. Catal.*, 2020, **3**, 274–288.
2 N. J. Claassens, C. A. Cotton, D. Kopljar and A. Bar-Even, *Nat. Catal.*, 2019, **2**, 437.
3 L. V. Teixeira, L. F. Moutinho and A. S. Romão-Dumaresq, *Biofuels Bioprod. Biorefining.*, 2018, **12**(6), 1103–1117.
4 S. Cestellos-Blanco, H. Zhang, J. M. Kim, Y.-X. Shen and P. Yang, *Nat. Catal.*, 2020, **3**, 245–255.
5 H. Zhang, H. Liu, Z. Tian, D. Lu, Y. Yu, S. Cestellos-Blanco, K. K. Sakimoto and P. Yang, *Nat. Nanotechnol.*, 2018, **13**, 900–905.
6 D. Karamanev, V. Pupkevich, K. Penev, V. Glibin, J. Gohil and V. Vajihinejad, *Energy*, 2017, **129**, 237–245.
7 F. Li, L. Chen, G. P. Knowles, D. R. MacFarlane and J. Zhang, *Angew. Chem., Int. Ed.*, 2017, **56**, 505–509.
8 J. Wu, M. Liu, P. P. Sharma, R. M. Yadav, L. Ma, Y. Yang, X. Zou, X.-D. Zhou, R. Vajtai and B. I. Yakobson, *Nano Lett.*, 2016, **16**, 466–470.
9 I. A. Figueroa, T. P. Barnum, P. Y. Somasekhar, C. I. Carlström, A. L. Engelbrektson and J. D. Coates, *Proc. Natl. Acad. Sci. U. S. A.*, 2018, **115**, 92–101.
10 X. Chen, Y. Cao, F. Li, Y. Tian and H. Song, *ACS Catal.*, 2018, **8**, 4429–4437.
11 S. Bajracharya, K. Vanbroekhoven, C. J.-N. Buisman, D. Strik and D. Pant, *Faraday Discuss.*, 2017, **202**, 433–449.
12 L. Jourdin, S. M. Raes, C. J. Buisman and D. P. Strik, *Front. Energy Res.*, 2018, **6**, 7.
13 T. Krieg, A. Sydow, S. Faust, I. Huth and D. Holtmann, *Angew. Chem., Int. Ed.*, 2018, **57**, 1879–1882.
14 Z. Sun, T. Ma, H. Tao, Q. Fan and B. Han, *Chem*, 2017, **3**, 560–587.
15 P.-L. Tremblay, L. T. Angenent and T. Zhang, *Trends Biotechnol.*, 2017, **35**, 360–371.
16 A. J. Garza, A. T. Bell and M. Head-Gordon, *ACS Catal.*, 2018, **8**, 1490–1499.
17 K. P. Kuhl, E. R. Cave, D. N. Abram and T. F. Jaramillo, *Energy Environ. Sci.*, 2012, **5**, 7050–7059.
18 M. D. Wodrich, B. Sawatlon, M. Busch and C. Corminboeuf, *Acc. Chem. Res.*, 2021, **54**, 1107–1117.
19 Y. Li and Q. Sun, *Adv. Energy Mater.*, 2016, **6**, 1600463.
20 A. A. Peterson and J. K. Nørskov, *J. Phys. Chem. Lett.*, 2012, **3**, 251–258.
21 W. Zhu, R. Michalsky, O. N. Metin, H. Lv, S. Guo, C. J. Wright, X. Sun, A. A. Peterson and S. Sun, *J. Am. Chem. Soc.*, 2013, **135**, 16833–16836.
22 Y. Lai, N. B. Watkins, A. Rosas-Hernández, A. Thevenon, G. P. Heim, L. Zhou, Y. Wu, J. C. Peters, J. M. Gregoire and T. Agapie, *ACS Cent. Sci.*, 2021, **7**, 1756–1762.
23 H. Shen, C. Choi, J. Masa, X. Li, J. Qiu, Y. Jung and Z. Sun, *Chem*, 2021, **7**, 1708–1754.
24 C. J. Bondue, M. Graf, A. Goyal and M. T. Koper, *J. Am. Chem. Soc.*, 2020, **143**, 279–285.
25 H.-Q. Liang, S. Zhao, X.-M. Hu, M. Ceccato, T. Skrydstrup and K. Daasbjerg, *ACS Catal.*, 2021, **11**, 958–966.
26 H. Tao, X. Sun, S. Back, Z. Han, Q. Zhu, A. W. Robertson, T. Ma, Q. Fan, B. Han and Y. Jung, *Chem. Sci.*, 2018, **9**, 483–487.
27 A. Schmid, J. Dordick, B. Hauer, A. Kiener, M. Wubbolts and B. Witholt, *Nature*, 2001, **409**, 258–268.
28 P. De Luna, C. Hahn, D. Higgins, S. A. Jaffer, T. F. Jaramillo and E. H. Sargent, *Science*, 2019, **364**(6438), eaav3506.
29 S. Schlager, A. Fuchsbauer, M. Haberbauer, H. Neugebauer and N. S. Sariciftci, *J. Mater. Chem. A*, 2017, **5**, 2429–2443.
30 N. J. Claassens, I. Sánchez-Andrea, D. Z. Sousa and A. Bar-Even, *Curr. Opin. Biotechnol*, 2018, **50**, 195–205.
31 D. E. Holmes, D. R. Bond and D. R. Lovley, *Appl. Environ. Microbiol.*, 2004, **70**, 1234–1237.
32 M. Yuan, M. J. Kummer and S. D. Minteer, *Chem. – Eur. J.*, 2019, **25**, 14258–14266.
33 E. Rosenberg, E. F. DeLong, S. Lory, E. Stackebrandt and F. Thompson, *The Prokaryotes*, Springer, New York, 2006.

34 D. T.-N. Nguyen, O. K. Lee, S. Hadiyati, A. N. Affifah, M. S. Kim and E. Y. Lee, *Metab. Eng.*, 2019, **54**, 170–179.
35 F. Sonntag, C. Kroner, P. Lubuta, R. Peyraud, A. Horst, M. Buchhaupt and J. Schrader, *Metab. Eng.*, 2015, **32**, 82–94.
36 C. M. Humphreys and N. P. Minton, *Curr. Opin. Biotechnol*, 2018, **50**, 174–181.
37 S. Nitopi, E. Bertheussen, S. B. Scott, X. Liu, A. K. Engstfeld, S. Horch, B. Seger, I. E.-L. Stephens, K. Chan, C. Hahn, J. K. Nørskov, T. F. Jaramillo and I. Chorkendorff, *Chem. Rev.*, 2019, **119**, 7610–7672.
38 F. Franco, C. Rettenmaier, H. S. Jeon and B. Roldan Cuenya, *Chem. Soc. Rev.*, 2020, **49**, 6884–6946.
39 L. Dai, Y. Xue, L. Qu, H.-J. Choi and J.-B. Baek, *Chem. Rev.*, 2015, **115**, 4823–4892.
40 A. Peigney, C. Laurent, E. Flahaut, R. Bacsa and A. Rousset, *Carbon*, 2001, **39**, 507–514.
41 M. Dresselhaus, *Phys. World*, 1996, **9**, 18.
42 P. Kang, S. Zhang, T. J. Meyer and M. Brookhart, *Angew. Chem., Int. Ed.*, 2014, **53**, 8709–8713.
43 H. Zhao, Y. Zhang, B. Zhao, Y. Chang and Z. Li, *Environ. Sci. Technol.*, 2012, **46**, 5198–5204.
44 J. Wu, R. M. Yadav, M. Liu, P. P. Sharma, C. S. Tiwary, L. Ma, X. Zou, X.-D. Zhou, B. I. Yakobson and J. Lou, *ACS Nano*, 2015, **9**, 5364–5371.
45 A. K. Geim and K. S. Novoselov, *Nanosci. Technol.*, World Scientific, 2010, pp. 11–19.
46 M. D. Stoller, S. Park, Y. Zhu, J. An and R. S. Ruoff, *Nano Lett.*, 2008, **8**, 3498–3502.
47 P. Han, X. Yu, D. Yuan, M. Kuang, Y. Wang, A. M. Al-Enizi and G. Zheng, *J. Colloid Interface Sci.*, 2019, **534**, 332–337.
48 K.-R. Kim, J. Kang and K.-J. Chae, *Int. J. Hydrogen Energ.*, 2017, **42**, 27623–27629.
49 H. Furukawa, K. E. Cordova, M. O'Keeffe and O. M. Yaghi, *Science*, 2013, **341**(6169), 1230444.
50 A. J. Howarth, Y. Liu, P. Li, Z. Li, T. C. Wang, J. T. Hupp and O. K. Farha, *Nat. Rev. Mater.*, 2016, **1**, 1–15.
51 T. Y. Ma, S. Dai, M. Jaroniec and S. Z. Qiao, *J. Am. Chem. Soc.*, 2014, **136**, 13925–13931.
52 D.-H. Nam, O. S. Bushuyev, J. Li, P. De Luna, A. Seifitokaldani, C.-T. Dinh, F. P. García de Arquer, Y. Wang, Z. Liang and A. H. Proppe, *J. Am. Chem. Soc.*, 2018, **140**, 11378–11386.
53 P. Deng, F. Yang, Z. Wang, S. Chen, Y. Zhou, S. Zaman and B. Y. Xia, *Angew. Chem.*, 2020, **132**, 10899–10905.
54 X.-F. Qiu, H.-L. Zhu, J.-R. Huang, P.-Q. Liao and X.-M. Chen, *J. Am. Chem. Soc.*, 2021, **143**, 7242–7246.
55 V. Uppada, S. Bhaduri and S. B. Noronha, *Curr. Sci.*, 2014, 946–957.
56 H. Zhao and W. A. Van Der Donk, *Curr. Opin. Biotechnol*, 2003, **14**, 583–589.
57 H. Chen, F. Dong and S. D. Minteer, *Nat. Catal.*, 2020, **3**, 225–244.
58 R. D. Milton and S. D. Minteer, *J. R. Soc., Interface*, 2017, **14**, 20170253.
59 U. Schröder, *Phys. Chem. Chem. Phys.*, 2007, **9**, 2619–2629.
60 M. T. Matsena and E. M.-N. Chirwa, *Biofuels and Bioenergy*, Elsevier, 2022, pp. 321–358.
61 X. Liu and X. Yu, *ACS Energy Lett.*, 2020, **5**, 867–878.
62 M. Muthuvel, X. Jin and G. Botte, *Encyclopedia of electrochemical power sources*, Elsevier, 2009, pp. 158–171.
63 H. Mistry, R. Reske, Z. Zeng, Z.-J. Zhao, J. Greeley, P. Strasser and B. R. Cuenya, *J. Am. Chem. Soc.*, 2014, **136**, 16473–16476.
64 J. Rosen, G. S. Hutchings, Q. Lu, S. Rivera, Y. Zhou, D. G. Vlachos and F. Jiao, *ACS Catal.*, 2015, **5**, 4293–4299.
65 F. Yang, A. O. Elnabawy, R. Schimmenti, P. Song, J. Wang, Z. Peng, S. Yao, R. Deng, S. Song and Y. Lin, *Nat. Commun.*, 2020, **11**, 1–8.
66 R. Zhang, W. Lv and L. Lei, *Appl. Surf. Sci.*, 2015, **356**, 24–29.
67 D. Liu, T. Zheng, C. Buisman and A. Ter Heijne, *ACS Sustainable Tain. Chen. Eng.*, 2017, **5**, 11346–11353.
68 C.-T. Dinh, T. Burdyny, M. G. Kibria, A. Seifitokaldani, C. M. Gabardo, F. P.-G. de Arquer, A. Kiani, J. P. Edwards, P. De Luna and O. S. Bushuyev, *Science*, 2018, **360**, 783–787.
69 Y. Kwon, Y. Lum, E. L. Clark, J. W. Ager and A. T. Bell, *ChemElectroChem*, 2016, **3**, 1012–1019.
70 A. Dutta, M. Rahaman, N. C. Luedi, M. Mohos and P. Broekmann, *ACS Catal.*, 2016, **6**, 3804–3814.
71 N. Hoshi, M. Kato and Y. Hori, *J. Electroanal. Chem.*, 1997, **440**, 283–286.
72 Q. Zhang, W. Xu, J. Xu, Y. Liu and J. Zhang, *Catal. Today*, 2018, **318**, 15–22.
73 M. Li, S. Garg, X. Chang, L. Ge, L. Li, M. Konarova, T. E. Rufford, V. Rudolph and G. Wang, *Small Methods*, 2020, **4**, 2000033.
74 W. Ye, X. Guo and T. Ma, *Chem. Eng. J.*, 2021, 128825.
75 S. Lee, D. Kim and J. Lee, *Angew. Chem.*, 2015, **127**, 14914–14918.
76 D. Cheng, Z.-J. Zhao, G. Zhang, P. Yang, L. Li, H. Gao, S. Liu, X. Chang, S. Chen, T. Wang, G. A. Ozin, Z. Liu and J. Gong, *Nat. Commun.*, 2021, **12**, 395.
77 W. Tang, A. A. Peterson, A. S. Varela, Z. P. Jovanov, L. Bech, W. J. Durand, S. Dahl, J. K. Nørskov and I. Chorkendorff, *Phys. Chem. Chem. Phys.*, 2012, **14**, 76–81.
78 P. De Luna, R. Quintero-Bermudez, C.-T. Dinh, M. B. Ross, O. S. Bushuyev, P. Todorović, T. Regier, S. O. Kelley, P. Yang and E. H. Sargent, *Nat. Catal.*, 2018, **1**, 103–110.
79 T. Burdyny, P. J. Graham, Y. Pang, C.-T. Dinh, M. Liu, E. H. Sargent and D. Sinton, *ACS Sustainable Tain. Chen. Eng.*, 2017, **5**, 4031–4040.
80 A. Klinkova, P. De Luna, C.-T. Dinh, O. Voznyy, E. M. Larin, E. Kumacheva and E. H. Sargent, *ACS Catal.*, 2016, **6**, 8115–8120.
81 M. Liu, Y. Pang, B. Zhang, P. De Luna, O. Voznyy, J. Xu, X. Zheng, C. T. Dinh, F. Fan and C. Cao, *Nature*, 2016, **537**, 382–386.
82 T. Saberi Safaei, A. Mepham, X. Zheng, Y. Pang, C.-T. Dinh, M. Liu, D. Sinton, S. O. Kelley and E. H. Sargent, *Nano Lett.*, 2016, **16**, 7224–7228.
83 T. Kim and G. T.-R. Palmore, *Nat. Commun.*, 2020, **11**, 1–11.

84 A. H. Anwer, N. Khan, M. D. Khan, M. Shahadat and M. Z. Khan, *J. Environ. Chem. Eng.*, 2021, 106650.
85 Y. Zhou, F. Che, M. Liu, C. Zou, Z. Liang, P. De Luna, H. Yuan, J. Li, Z. Wang and H. Xie, *Nat. Chem.*, 2018, **10**, 974–980.
86 J. Christophe, T. Doneux and C. Buess-Herman, *Electrocatalysis*, 2012, **3**, 139–146.
87 S. Ma, M. Sadakiyo, M. Heima, R. Luo, R. T. Haasch, J. I. Gold, M. Yamauchi and P. J.-A. Kenis, *J. Am. Chem. Soc.*, 2017, **139**, 47–50.
88 Z. Huang, J. Gong and Z. Nie, *Acc. Chem. Res.*, 2019, **52**, 1125–1133.
89 H. Li, S. Zha, Z.-J. Zhao, H. Tian, S. Chen, Z. Gong, W. Cai, Y. Wang, Y. Cui, L. Zeng, R. Mu and J. Gong, *ACS Catal.*, 2018, **8**, 5526–5532.
90 A. Guan, C. Yang, Y. Quan, H. Shen, N. Cao, T. Li, Y. Ji and G. Zheng, *Chem. – Asian J.*, 2019, **14**, 3969–3980.
91 S. Sun, H. Cheng, X. Li, X. Wu, D. Zhen, Y. Wang, R. Jin and G. He, *Ind. Eng. Chem. Res.*, 2021, **60**, 1164–1174.
92 L. Hu, Y. Zhang and W. Han, *New J. Chem.*, 2019, **43**, 3269–3272.
93 T. Wang, J. Yang, J. Chen, Q. He, Z. Li, L. Lei, J. Lu, M. K. Leung, B. Yang and Y. Hou, *Chin. Chem. Lett.*, 2020, **31**, 1438–1442.
94 M. Zhu, J. Chen, L. Huang, R. Ye, J. Xu and Y. F. Han, *Angew. Chem., Int. Ed.*, 2019, **58**, 6595–6599.
95 G. Zhen, X. Lu, T. Kobayashi, G. Kumar and K. Xu, *Chem. Eng. J.*, 2016, **284**, 1146–1155.
96 X. Li, S. Wang, L. Li, X. Zu, Y. Sun and Y. Xie, *Acc. Chem. Res.*, 2020, **53**, 2964–2974.
97 R. Geioushy, M. M. Khaled, K. Alhooshani, A. S. Hakeem and A. Rinaldi, *Electrochim. Acta*, 2017, **245**, 456–462.
98 A. A. Ensafi, H. A. Alinajafi and B. Rezaei, *J. Electroanal. Chem.*, 2016, **783**, 82–89.
99 J. Yuan, M.-P. Yang, W.-Y. Zhi, H. Wang, H. Wang and J.-X. Lu, *J. CO2 Util.*, 2019, **33**, 452–460.
100 J. Yuan, W.-Y. Zhi, L. Liu, M.-P. Yang, H. Wang and J.-X. Lu, *Electrochim. Acta*, 2018, **282**, 694–701.
101 P. Sekar, L. Calvillo, C. Tubaro, M. Baron, A. Pokle, F. Carraro, A. Martucci and S. Agnoli, *ACS Catal.*, 2017, **7**, 7695–7703.
102 Z. Cai, Y. Zhang, Y. Zhao, Y. Wu, W. Xu, X. Wen, Y. Zhong, Y. Zhang, W. Liu and H. Wang, *Nano Res.*, 2019, **12**, 345–349.
103 F. Lei, W. Liu, Y. Sun, J. Xu, K. Liu, L. Liang, T. Yao, B. Pan, S. Wei and Y. Xie, *Nat. Commun.*, 2016, **7**, 1–8.
104 K. Ye, Z. Zhou, J. Shao, L. Lin, D. Gao, N. Ta, R. Si, G. Wang and X. Bao, *Angew. Chem., Int. Ed.*, 2020, **59**, 4814–4821.
105 Q. Zhu, X. Sun, D. Yang, J. Ma, X. Kang, L. Zheng, J. Zhang, Z. Wu and B. Han, *Nat. Commun.*, 2019, **10**, 1–11.
106 E. Nwanebu, S. Omanovic, S. Hrapovic, A. G. Vidales and B. Tartakovsky, *Int. J. Hydrogen Energy*, 2021, **47**(1), 203–215.
107 Z. Chen, K. Mou, S. Yao and L. Liu, *J. Mater. Chem. A*, 2018, **6**, 11236–11243.
108 C. Hu, R. Paul, Q. Dai and L. Dai, *Chem. Soc. Rev.*, 2021, **50**, 11785–11843.
109 D. Gao, H. Zhou, J. Wang, S. Miao, F. Yang, G. Wang, J. Wang and X. Bao, *J. Am. Chem. Soc.*, 2015, **137**, 4288–4291.
110 G. Zhang, Z. J. Zhao, D. Cheng, H. Li, J. Yu, Q. Wang, H. Gao, J. Guo, H. Wang, G. A. Ozin, T. Wang and J. Gong, *Nat. Commun.*, 2021, **12**, 5745.
111 S. Kattel, P. J. Ramírez, J. G. Chen, J. A. Rodriguez and P. Liu, *Science*, 2017, **355**, 1296–1299.
112 Z. Wang, G. Yang, Z. Zhang, M. Jin and Y. Yin, *ACS Nano*, 2016, **10**, 4559–4564.
113 D. H. Won, H. Shin, J. Koh, J. Chung, H. S. Lee, H. Kim and S. I. Woo, *Angew. Chem.*, 2016, **128**, 9443–9446.
114 Z. Li, Y. Yang, Z. Yin, X. Wei, H. Peng, K. Lyu, F. Wei, L. Xiao, G. Wang and H. D. Abruna, *ACS Catal.*, 2021, **11**, 2473–2482.
115 G. Dunfeng, W. Pengfei, L. Hefei, L. Long, W. Guoxiong and B. Xinhe, *Acta Phys. Sin.*, 2021, **37**(5), 2009021.
116 S. Verma, B. Kim, H. R.-M. Jhong, S. Ma and P. J. Kenis, *ChemSusChem*, 2016, **9**, 1972–1979.
117 D. T. Whipple, E. C. Finke and P. J. Kenis, *Electrochem. Solid-State Lett.*, 2010, **13**, B109.
118 Y. Yang and F. Li, *Curr. Opin. Green Sustain.*, 2021, **27**, 100419.
119 C. M. Gabardo, C. P. O'Brien, J. P. Edwards, C. McCallum, Y. Xu, C.-T. Dinh, J. Li, E. H. Sargent and D. Sinton, *Joule*, 2019, **3**, 2777–2791.
120 F. Li, A. Thevenon, A. Rosas-Hernández, Z. Wang, Y. Li, C. M. Gabardo, A. Ozden, C. T. Dinh, J. Li and Y. Wang, *Nature*, 2020, **577**, 509–513.
121 B. Endrodi, E. Kecsenovity, A. Samu, F. Darvas, R. Jones, V. Török, A. Danyi and C. Janáky, *ACS Energy Lett.*, 2019, **4**, 1770–1777.
122 X. Tan, C. Yu, Y. Ren, S. Cui, W. Li and J. Qiu, *Energy Environ. Sci.*, 2021, **14**, 765–780.
123 H. Chen, O. Simoska, K. Lim, M. Grattieri, M. Yuan, F. Dong, Y. S. Lee, K. Beaver, S. Weliwatte and E. M. Gaffney, *Chem. Rev.*, 2020, **120**, 12903–12993.
124 M. Miller, W. E. Robinson, A. R. Oliveira, N. Heidary, N. Kornienko, J. Warnan, I. A. Pereira and E. Reisner, *Angew. Chem., Int. Ed.*, 2019, **58**, 4601–4605.
125 C. Cadoux and R. D. Milton, *ChemElectroChem*, 2020, **7**, 1974–1986.
126 D. Leech, P. Kavanagh and W. Schuhmann, *Electrochim. Acta*, 2012, **84**, 223–234.
127 D. P. Hickey, E. M. Gaffney and S. D. Minteer, *Top Curr. Chem. (Cham)*, 2018, **376**, 43.
128 X. Ji, Z. Su, P. Wang, G. Ma and S. Zhang, *Small*, 2016, **12**, 4753–4762.
129 Y. Li, L. Wen, T. Tan and Y. Lv, *Front. Bioeng. Biotechnol.*, 2019, **7**, 394.
130 S. Amanullah, P. Saha, A. Nayek, M. Ahmed and A. Dey, *Chem. Soc. Rev.*, 2021, **50**, 3755–3823.
131 F. Mayer, F. Enzmann, A. M. Lopez and D. Holtmann, *Bioresour. Technol.*, 2019, **289**, 121706.
132 M. Schulman, D. Parker, L. G. Ljungdahl and H. G. Wood, *J. Bacteriol. Parasitol*, 1972, **109**, 633–644.

133 M. Calvin and A. A. Benson, *Science*, 1948, **107**, 476.
134 H. Huber, M. Gallenberger, U. Jahn, E. Eylert, I. A. Berg, D. Kockelkorn, W. Eisenreich and G. Fuchs, *Proc. Natl. Acad. Sci. U. S. A.*, 2008, **105**, 7851–7856.
135 M. Evans, B. B. Buchanan and D. I. Arnon, *Proc. Natl. Acad. Sci. U. S. A.*, 1966, **55**, 928–934.
136 M. Hügler, H. Huber, K. O. Stetter and G. Fuchs, *Arch. Microbiol.*, 2003, **179**, 160–173.
137 H. Holo, *Arch. Microbiol.*, 1989, **151**, 252–256.
138 T. Schwander, L. Schada von Borzyskowski, S. Burgener, N. S. Cortina and T. J. Erb, *Science*, 2016, **354**, 900.
139 S. Luo, P. P. Lin, L.-Y. Nieh, G.-B. Liao, P.-W. Tang, C. Chen and J. C. Liao, *Nat. Catal.*, 2022, **5**, 154–162.
140 L. Xiao, G. Liu, F. Gong, H. Zhu, Y. Zhang, Z. Cai and Y. Li, *ACS Catal.*, 2021, **12**, 799–808.
141 G. Hu, Z. Li, D. Ma, C. Ye, L. Zhang, C. Gao, L. Liu and X. Chen, *Nat. Catal.*, 2021, **4**, 395–406.
142 W. B. Whitaker, J. A. Jones, R. K. Bennett, J. E. Gonzalez, V. R. Vernacchio, S. M. Collins, M. A. Palmer, S. Schmidt, M. R. Antoniewicz and M. A. Koffas, *Metab. Eng.*, 2017, **39**, 49–59.
143 F. Guo, Z. Dai, W. Peng, S. Zhang, J. Zhou, J. Ma, W. Dong, F. Xin, W. Zhang and M. Jiang, *Biotechnol. Bioeng.*, 2021, **118**, 357–371.
144 N. J. Claassens, H. He and A. Bar-Even, *Curr. Issues Mol. Biol.*, 2019, **33**, 237–248.
145 M. Kumar, S. Sundaram, E. Gnansounou, C. Larroche and I. S. Thakur, *Bioresour. Technol.*, 2018, **247**, 1059–1068.
146 M. Calvin and A. A. Benson, *Science*, 1949, **109**, 140–142.
147 S. Gleizer, R. Ben-Nissan, Y. M. Bar-On, N. Antonovsky, E. Noor, Y. Zohar, G. Jona, E. Krieger, M. Shamshoum, A. Bar-Even and R. Milo, *Cell*, 2019, **179**, 1255–1263.
148 J. Bang, C. H. Hwang, J. H. Ahn, J. A. Lee and S. Y. Lee, *Nat. Microbiol.*, 2020, **5**, 1459–1463.
149 R. Ganigué, S. Puig, P. Batlle-Vilanova, M. D. Balaguer and J. Colprim, *Chem. Commun.*, 2015, **51**, 3235–3238.
150 T. Krieg, A. Sydow, S. Faust, I. Huth and D. Holtmann, *Angew. Chem., Int. Ed. Engl.*, 2018, **57**, 1879–1882.
151 J. Yang, S. Sun, Y. Men, Y. Zeng, Y. Zhu, Y. Sun and Y. Ma, *Catal. Sci. Technol.*, 2017, **7**, 3459–3463.
152 S. Sundaram, C. Diehl, N. S. Cortina, J. Bamberger, N. Paczia and T. J. Erb, *Angew. Chem., Int. Ed. Engl.*, 2021, **60**, 16420–16425.
153 C. Chen, Y. Li, S. Yu, S. Louisia, J. Jin, M. Li, M. B. Ross and P. Yang, *Joule*, 2020, **4**, 1688–1699.
154 H. Wu, H. Pan, Z. Li, T. Liu, F. Liu, S. Xiu, J. Wang, H. Wang, Y. Hou and B. Yang, *Chem. Eng. J.*, 2022, **430**, 132943.
155 S. Bolognesi, L. Bañeras, E. Perona-Vico, A. G. Capodaglio, M. D. Balaguer and S. Puig, *Sustain. Energy Fuels*, 2022, **6**, 150–161.
156 A. L. Ghindilis, P. Atanasov and E. Wilkins, *Electroanalysis*, 1997, **9**, 661–674.
157 M. Yuan, S. Sahin, R. Cai, S. Abdellaoui, D. P. Hickey, S. D. Minteer and R. D. Milton, *Angew. Chem.*, 2018, **130**, 6692–6696.
158 O. Bretschger, K. Carpenter, T. Phan, S. Suzuki, S. I. Ishii, E. Grossi-Soyster, M. Flynn and J. Hogan, *Bioresour. Technol*, 2015, **195**, 254–264.
159 C. Liu, B. C. Colón, M. Ziesack, P. A. Silver and D. G. Nocera, *Science*, 2016, **352**, 1210–1213.
160 H. M. Woo, *Curr. Opin. Biotechnol*, 2017, **45**, 1–7.
161 H. Li, P. H. Opgenorth, D. G. Wernick, S. Rogers, T.-Y. Wu, W. Higashide, P. Malati, Y.-X. Huo, K. M. Cho and J. C. Liao, *Science*, 2012, **335**, 1596.
162 J. A. Cornejo, H. Sheng, E. Edri, C. Ajo-Franklin and H. Frei, *Nat. Commun.*, 2018, **9**, 2263.
163 T. Haas, R. Krause, R. Weber, M. Demler and G. Schmid, *Nat. Catal.*, 2018, **1**, 32.
164 R. M. Rodrigues, X. Guan, J. A. Iñiguez, D. A. Estabrook, J. O. Chapman, S. Huang, E. M. Sletten and C. Liu, *Nat. Catal.*, 2019, **2**, 407–414.
165 F. Rudroff, M. D. Mihovilovic, H. Gröger, R. Snajdrova, H. Iding and U. T. Bornscheuer, *Nat. Catal.*, 2018, **1**, 12–22.
166 J. Guo, M. Suástegui, K. K. Sakimoto, V. M. Moody, G. Xiao, D. G. Nocera and N. S. Joshi, *Science*, 2018, **362**, 813–816.
167 A. Ruff, F. Conzuelo and W. Schuhmann, *Nat. Catal.*, 2020, **3**, 214–224.
168 L. Xu, Y. Xiu, F. Liu, Y. Liang and S. Wang, *Molecules*, 2020, **25**, 3653.
169 R. E. Sharp and S. K. Chapman, *Biochim. Biophys. Acta*, 1999, **1432**, 143–158.
170 C. C. Page, C. C. Moser, X. Chen and P. L. Dutton, *Nature*, 1999, **402**, 47–52.
171 J. T. Holland, C. Lau, S. Brozik, P. Atanassov and S. Banta, *J. Am. Chem. Soc.*, 2011, **133**, 19262–19265.
172 K. Xiang, Y. Qiao, C. B. Ching and C. M. Li, *Electrochem. Commun.*, 2009, **11**, 1593–1595.
173 N.-M. D. Courchesne, E. P. DeBenedictis, J. Tresback, J. J. Kim, A. Duraj-Thatte, D. Zanuy, S. Keten and N. S. Joshi, *Nanotechnology*, 2018, **29**, 454002.
174 P. Q. Nguyen, Z. Botyanszki, P. K.-R. Tay and N. S. Joshi, *Nat. Commun.*, 2014, **5**, 1–10.
175 D. R. Lovley and J. Yao, *Trends Biotechnol.*, 2021, **39**, 940–952.
176 F. Wang, Y. Gu, J. P. O'Brien, M. Y. Sophia, S. E. Yalcin, V. Srikanth, C. Shen, D. Vu, N. L. Ing and A. I. Hochbaum, *Cell*, 2019, **177**, 361–369.e310.
177 S. E. Yalcin, J. P. O'Brien, Y. Gu, K. Reiss, S. M. Yi, R. Jain, V. Srikanth, P. J. Dahl, W. Huynh, D. Vu, A. Acharya, S. Chaudhuri, T. Varga, V. S. Batista and N. S. Malvankar, *Nat. Chem. Biol.*, 2020, 1136–1142Medium: ED; Size.
178 F. J. Meysman, R. Cornelissen, S. Trashin, R. Bonné, S. H. Martinez, J. van der Veen, C. J. Blom, C. Karman, J.-L. Hou and R. T. Eachambadi, *Nat. Commun.*, 2019, **10**, 1–8.
179 K. U. Kjeldsen, L. Schreiber, C. A. Thorup, T. Boesen, J. T. Bjerg, T. Yang, M. S. Dueholm, S. Larsen, N. Risgaard-Petersen and M. Nierychlo, *Proc. Natl. Acad. Sci. U. S. A.*, 2019, **116**, 19116–19125.
180 M. J. Edwards, G. F. White, J. N. Butt, D. J. Richardson and T. A. Clarke, *Cell*, 2020, **181**, 665–673.e610.

181 J. Zhao, F. Li, Y. Cao, X. Zhang, T. Chen, H. Song and Z. Wang, *Biotechnol. Adv.*, 2020, 107682.
182 M. A. Thirumurthy and A. K. Jones, *Nanotechnology*, 2020, **31**, 124001.
183 E. M. Nichols, J. J. Gallagher, C. Liu, Y. Su, J. Resasco, Y. Yu, Y. Sun, P. Yang, M. C.-Y. Chang and C. J. Chang, *Proc. Natl. Acad. Sci. U. S. A.*, 2015, **112**, 11461–11466.
184 F. Li, Y.-X. Li, Y.-X. Cao, L. Wang, C.-G. Liu, L. Shi and H. Song, *Nat. Commun.*, 2018, **9**, 1–13.
185 Y. Yang, Y. Ding, Y. Hu, B. Cao, S. A. Rice, S. Kjelleberg and H. Song, *ACS Synth. Biol.*, 2015, **4**, 815–823.
186 A. Goyal, G. Marcandalli, V. A. Mints and M. T. Koper, *J. Am. Chem. Soc.*, 2020, **142**, 4154–4161.
187 S. Zhao, N. Austin, M. Li, Y. Song, S. D. House, S. Bernhard, J. C. Yang, G. Mpourmpakis and R. Jin, *ACS Catal.*, 2018, **8**, 4996–5001.
188 S. Chu, S. Fan, Y. Wang, D. Rossouw, Y. Wang, G. A. Botton and Z. Mi, *Angew. Chem., Int. Ed.*, 2016, **55**, 14262–14266.
189 Y.-C. Hsieh, S. D. Senanayake, Y. Zhang, W. Xu and D. E. Polyansky, *ACS Catal.*, 2015, **5**, 5349–5356.
190 D. Gao, H. Zhou, F. Cai, D. Wang, Y. Hu, B. Jiang, W.-B. Cai, X. Chen, R. Si and F. Yang, *Nano Res.*, 2017, **10**, 2181–2191.
191 X. Min and M. W. Kanan, *J. Am. Chem. Soc.*, 2015, **137**, 4701–4708.
192 B. Qin, H. Wang, F. Peng, H. Yu and Y. Cao, *J. CO2 Util.*, 2017, **21**, 219–223.
193 R. Kas, K. K. Hummadi, R. Kortlever, P. De Wit, A. Milbrat, M. W. Luiten-Olieman, N. E. Benes, M. T. Koper and G. Mul, *Nat. Commun.*, 2016, **7**, 1–7.
194 R. Daiyan, X. Lu, Y. H. Ng and R. Amal, *ChemistrySelect*, 2017, **2**, 879–884.
195 D. Raciti, Y. Wang, J. H. Park and C. Wang, *ACS Appl. Energy Mater.*, 2018, **1**, 2392–2398.
196 J. Rosen, G. S. Hutchings, Q. Lu, R. V. Forest, A. Moore and F. Jiao, *ACS Catal.*, 2015, **5**, 4586–4591.
197 K. Fan, Y. Jia, Y. Ji, P. Kuang, B. Zhu, X. Liu and J. Yu, *ACS Catal.*, 2019, **10**, 358–364.
198 P. Lu, D. Gao, H. He, Q. Wang, Z. Liu, S. Dipazir, M. Yuan, W. Zu and G. Zhang, *Nanoscale*, 2019, **11**, 7805–7812.
199 J. Qu, X. Zhang, Y. Wang and C. Xie, *Electrochim. Acta*, 2005, **50**, 3576–3580.
200 D. Gao, Y. Zhang, Z. Zhou, F. Cai, X. Zhao, W. Huang, Y. Li, J. Zhu, P. Liu and F. Yang, *J. Am. Chem. Soc.*, 2017, **139**, 5652–5655.
201 Y. Chen, C. W. Li and M. W. Kanan, *J. Am. Chem. Soc.*, 2012, **134**, 19969–19972.
202 L.-P. Yuan, W.-J. Jiang, X.-L. Liu, Y.-H. He, C. He, T. Tang, J. Zhang and J.-S. Hu, *ACS Catal.*, 2020, **10**, 13227–13235.
203 J. Wang, G. Wang, J. Zhang, Y. Wang, H. Wu, X. Zheng, J. Ding, X. Han, Y. Deng and W. Hu, *Angew. Chem., Int. Ed.*, 2021, **60**, 7602–7606.
204 D. Wu, G. Huo, W. Chen, X.-Z. Fu and J.-L. Luo, *Appl. Catal., B*, 2020, **271**, 118957.
205 R. Kortlever, I. Peters, S. Koper and M. T. Koper, *ACS Catal.*, 2015, **5**, 3916–3923.
206 D. Kim, J. Resasco, Y. Yu, A. M. Asiri and P. Yang, *Nat. Commun.*, 2014, **5**, 1–8.
207 Y. Wang, L. Cao, N. J. Libretto, X. Li, C. Li, Y. Wan, C. He, J. Lee, J. Gregg and H. Zong, *J. Am. Chem. Soc.*, 2019, **141**, 16635–16642.
208 R. Lin, X. Ma, W.-C. Cheong, C. Zhang, W. Zhu, J. Pei, K. Zhang, B. Wang, S. Liang and Y. Liu, *Nano Res.*, 2019, **12**, 2866–2871.
209 J. Fu, W. Zhu, Y. Chen, Z. Yin, Y. Li, J. Liu, H. Zhang, J. J. Zhu and S. Sun, *Angew. Chem.*, 2019, **131**, 14238–14241.
210 X. Guo, Y. Zhang, C. Deng, X. Li, Y. Xue, Y.-M. Yan and K. Sun, *Chem. Commun.*, 2015, **51**, 1345–1348.
211 S. Sarfraz, A. T. Garcia-Esparza, A. Jedidi, L. Cavallo and K. Takanabe, *ACS Catal.*, 2016, **6**, 2842–2851.
212 M. Asadi, K. Kim, C. Liu, A. V. Addepalli, P. Abbasi, P. Yasaei, P. Phillips, A. Behranginia, J. M. Cerrato and R. Haasch, *Science*, 2016, **353**, 467–470.
213 Y. J. Jang, J.-W. Jang, J. Lee, J. H. Kim, H. Kumagai, J. Lee, T. Minegishi, J. Kubota, K. Domen and J. S. Lee, *Energy Environ. Sci.*, 2015, **8**, 3597–3604.
214 T. T. Hoang, S. Verma, S. Ma, T. T. Fister, J. Timoshenko, A. I. Frenkel, P. J. Kenis and A. A. Gewirth, *J. Am. Chem. Soc.*, 2018, **140**, 5791–5797.
215 D. Ren, B. S.-H. Ang and B. S. Yeo, *ACS Catal.*, 2016, **6**, 8239–8247.
216 S. Zhang, P. Kang, S. Ubnoske, M. K. Brennaman, N. Song, R. L. House, J. T. Glass and T. J. Meyer, *J. Am. Chem. Soc.*, 2014, **136**, 7845–7848.
217 C. Zhao, Z. Yin and J. Wang, *ChemElectroChem*, 2015, **2**, 1974–1982.
218 Y. Cheng, S. Zhao, B. Johannessen, J. P. Veder, M. Saunders, M. R. Rowles, M. Cheng, C. Liu, M. F. Chisholm and R. De Marco, *Adv. Mater.*, 2018, **30**, 1706287.
219 S. Huo, Z. Weng, Z. Wu, Y. Zhong, Y. Wu, J. Fang and H. Wang, *ACS Appl. Mater. Interfaces*, 2017, **9**, 28519–28526.
220 T. N. Huan, P. Prakash, P. Simon, G. Rousse, X. Xu, V. Artero, E. Gravel, E. Doris and M. Fontecave, *ChemSusChem*, 2016, **9**, 2317–2320.
221 X. Lu, T. H. Tan, Y. H. Ng and R. Amal, *Chem. – Eur. J.*, 2016, **22**, 11991–11996.
222 P. P. Sharma, J. Wu, R. M. Yadav, M. Liu, C. J. Wright, C. S. Tiwary, B. I. Yakobson, J. Lou, P. M. Ajayan and X. D. Zhou, *Angew. Chem., Int. Ed.*, 2015, **54**, 13701–13705.
223 X. Cui, Z. Pan, L. Zhang, H. Peng and G. Zheng, *Adv. Energy Mater.*, 2017, **7**, 1701456.
224 F. Pan, H. Zhao, W. Deng, X. Feng and Y. Li, *Electrochim. Acta*, 2018, **273**, 154–161.
225 W. Zheng, C. Guo, J. Yang, F. He, B. Yang, Z. Li, L. Lei, J. Xiao, G. Wu and Y. Hou, *Carbon*, 2019, **150**, 52–59.
226 B. Qin, Y. Li, H. Wang, G. Yang, Y. Cao, H. Yu, Q. Zhang, H. Liang and F. Peng, *Nano Energy*, 2019, **60**, 43–51.
227 S. Liu, H. B. Yang, S. F. Hung, J. Ding, W. Cai, L. Liu, J. Gao, X. Li, X. Ren and Z. Kuang, *Angew. Chem., Int. Ed.*, 2020, **59**, 798–803.
228 H. R.-M. Jhong, C. E. Tornow, C. Kim, S. Verma, J. L. Oberst, P. S. Anderson, A. A. Gewirth, T. Fujigaya,

N. Nakashima and P. J. Kenis, *ChemPhysChem*, 2017, **18**, 3274–3279.
229 M. Zhu, J. Chen, R. Guo, J. Xu, X. Fang and Y.-F. Han, *Appl. Catal., B*, 2019, **251**, 112–118.
230 H. Wang, J. Jia, P. Song, Q. Wang, D. Li, S. Min, C. Qian, L. Wang, Y. F. Li and C. Ma, *Angew. Chem., Int. Ed.*, 2017, **56**, 7847–7852.
231 P. Su, K. Iwase, S. Nakanishi, K. Hashimoto and K. Kamiya, *Small*, 2016, **12**, 6083–6089.
232 A. S. Varela, M. Kroschel, N. D. Leonard, W. Ju, J. Steinberg, A. Bagger, J. Rossmeisl and P. Strasser, *ACS Energy Lett.*, 2018, **3**, 812–817.
233 Q. Li, W. Zhu, J. Fu, H. Zhang, G. Wu and S. Sun, *Nano Energy*, 2016, **24**, 1–9.
234 L. Zeng, J. Shi, J. Luo and H. Chen, *J. Power Sources*, 2018, **398**, 83–90.
235 Z. Zhang, F. Ahmad, W. Zhao, W. Yan, W. Zhang, H. Huang, C. Ma and J. Zeng, *Nano Lett.*, 2019, **19**, 4029–4034.
236 J. Huang, X. Guo, G. Yue, Q. Hu and L. Wang, *ACS Appl. Mater. Interfaces*, 2018, **10**, 44403–44414.
237 B. Zhang, Z. Guo, Z. Zuo, W. Pan and J. Zhang, *Appl. Catal., B*, 2018, **239**, 441–449.
238 J. Wang, X. Huang, S. Xi, J. M. Lee, C. Wang, Y. Du and X. Wang, *Angew. Chem., Int. Ed.*, 2019, **58**, 13532–13539.
239 J. Choi, P. Wagner, S. Gambhir, R. Jalili, D. R. MacFarlane, G. G. Wallace and D. L. Officer, *ACS Energy Lett.*, 2019, **4**, 666–672.
240 H. Zhang, J. Li, S. Xi, Y. Du, X. Hai, J. Wang, H. Xu, G. Wu, J. Zhang and J. Lu, *Angew. Chem.*, 2019, **131**, 15013–15018.
241 J. Choi, P. Wagner, R. Jalili, J. Kim, D. R. MacFarlane, G. G. Wallace and D. L. Officer, *Adv. Energy Mater.*, 2018, **8**, 1801280.
242 W. Bi, X. Li, R. You, M. Chen, R. Yuan, W. Huang, X. Wu, W. Chu, C. Wu and Y. Xie, *Adv. Mater.*, 2018, **30**, 1706617.
243 J. Wang, L. Gan, Q. Zhang, V. Reddu, Y. Peng, Z. Liu, X. Xia, C. Wang and X. Wang, *Adv. Energy Mater.*, 2019, **9**, 1803151.
244 C. Zhang, S. Yang, J. Wu, M. Liu, S. Yazdi, M. Ren, J. Sha, J. Zhong, K. Nie and A. S. Jalilov, *Adv. Energy Mater.*, 2018, **8**, 1703487.
245 X. Li, W. Bi, M. Chen, Y. Sun, H. Ju, W. Yan, J. Zhu, X. Wu, W. Chu and C. Wu, *J. Am. Chem. Soc.*, 2017, **139**, 14889–14892.
246 C. Rogers, W. S. Perkins, G. Veber, T. E. Williams, R. R. Cloke and F. R. Fischer, *J. Am. Chem. Soc.*, 2017, **139**, 4052–4061.
247 J. Choi, J. Kim, P. Wagner, S. Gambhir, R. Jalili, S. Byun, S. Sayyar, Y. M. Lee, D. R. MacFarlane and G. G. Wallace, *Energy Environ. Sci.*, 2019, **12**, 747–755.
248 K. Zhao, Y. Liu, X. Quan, S. Chen and H. Yu, *ACS Appl. Mater. Interfaces*, 2017, **9**, 5302–5311.
249 J. Wu, S. Ma, J. Sun, J. I. Gold, C. Tiwary, B. Kim, L. Zhu, N. Chopra, I. N. Odeh and R. Vajtai, *Nat. Commun.*, 2016, **7**, 1–6.
250 Y. Pan, R. Lin, Y. Chen, S. Liu, W. Zhu, X. Cao, W. Chen, K. Wu, W.-C. Cheong and Y. Wang, *J. Am. Chem. Soc.*, 2018, **140**, 4218–4221.
251 F. Pan, H. Zhang, K. Liu, D. Cullen, K. More, M. Wang, Z. Feng, G. Wang, G. Wu and Y. Li, *ACS Catal.*, 2018, **8**, 3116–3122.
252 Q. Feng, S. Liu, X. Wang and G. Jin, *Appl. Surf. Sci.*, 2012, **258**, 5005–5009.
253 H. W. Shafaque, C. Lee, K. F. Fahy, J. K. Lee, J. M. LaManna, E. Baltic, D. S. Hussey, D. L. Jacobson and A. Bazylak, *ACS Appl. Mater. Interfaces*, 2020, **12**, 54585–54595.
254 B. Endrodi, E. Kecsenovity, A. Samu, F. Darvas, R. V. Jones, V. Torok, A. Danyi and C. Janaky, *ACS Energy Lett.*, 2019, **4**, 1770–1777.
255 S. Ren, D. Joulié, D. Salvatore, K. Torbensen, M. Wang, M. Robert and P. Berlinguette Curtis, *Science*, 2019, **365**, 367–369.
256 T. Zheng, K. Jiang, N. Ta, Y. Hu, J. Zeng, J. Liu and H. Wang, *Joule*, 2019, **3**, 265–278.
257 D. Kim, W. Choi, H. W. Lee, S. Y. Lee, Y. Choi, D. K. Lee, W. Kim, J. Na, U. Lee, Y. J. Hwang and D. H. Won, *ACS Energy Lett.*, 2021, **6**, 3488–3495.
258 G. O. Larrazabal, P. Strom-Hansen, J. P. Heli, K. Zeiter, K. T. Therkildsen, I. Chorkendorff and B. Seger, *ACS Appl. Mater. Interfaces*, 2019, **11**, 41281–41288.
259 L. Li, A. Ozden, S. Guo, A. D.-A. F.-P. Garci, C. Wang, M. Zhang, J. Zhang, H. Jiang, W. Wang, H. Dong, D. Sinton, E. H. Sargent and M. Zhong, *Nat. Commun.*, 2021, **12**, 5223.
260 C. Xia, P. Zhu, Q. Jiang, Y. Pan, W. Liang, E. Stavitski, H. N. Alshareef and H. Wang, *Nat. Energy*, 2019, **4**, 776–785.
261 Y. Xu, F. Li, A. Xu, J. P. Edwards, S. F. Hung, C. M. Gabardo, C. P. O'Brien, S. Liu, X. Wang, Y. Li, J. Wicks, R. K. Miao, Y. Liu, J. Li, J. E. Huang, J. Abed, Y. Wang, E. H. Sargent and D. Sinton, *Nat. Commun.*, 2021, **12**, 2932.
262 F. Li, Y. C. Li, Z. Wang, J. Li, D.-H. Nam, Y. Lum, M. Luo, X. Wang, A. Ozden, S.-F. Hung, B. Chen, Y. Wang, J. Wicks, Y. Xu, Y. Li, C. M. Gabardo, C.-T. Dinh, Y. Wang, T.-T. Zhuang, D. Sinton and E. H. Sargent, *Nat. Catal.*, 2019, **3**, 75–82.
263 X. Wang, Z. Wang, F. P. García de Arquer, C.-T. Dinh, A. Ozden, Y. C. Li, D.-H. Nam, J. Li, Y.-S. Liu, J. Wicks, Z. Chen, M. Chi, B. Chen, Y. Wang, J. Tam, J. Y. Howe, A. Proppe, P. Todorović, F. Li, T.-T. Zhuang, C. M. Gabardo, A. R. Kirmani, C. McCallum, S.-F. Hung, Y. Lum, M. Luo, Y. Min, A. Xu, C. P. O'Brien, B. Stephen, B. Sun, A. H. Ip, L. J. Richter, S. O. Kelley, D. Sinton and E. H. Sargent, *Nat. Energy*, 2020, **5**, 478–486.
264 F. Li, A. Thevenon, A. Rosas-Hernandez, Z. Wang, Y. Li, C. M. Gabardo, A. Ozden, C. T. Dinh, J. Li, Y. Wang, J. P. Edwards, Y. Xu, C. McCallum, L. Tao, Z. Q. Liang, M. Luo, X. Wang, H. Li, C. P. O'Brien, C. S. Tan, D. H. Nam, R. Quintero-Bermudez, T. T. Zhuang, Y. C. Li, Z. Han, R. D. Britt, D. Sinton, T. Agapie, J. C. Peters and E. H. Sargent, *Nature*, 2020, **577**, 509–513.
265 A. Ozden, F. Li, F. P. García de Arquer, A. Rosas-Hernández, A. Thevenon, Y. Wang, S.-F. Hung, X. Wang, B. Chen, J. Li, J. Wicks, M. Luo, Z. Wang, T. Agapie,

J. C. Peters, E. H. Sargent and D. Sinton, *ACS Energy Lett.*, 2020, **5**, 2811–2818.
266 J. Li, A. Ozden, M. Wan, Y. Hu, F. Li, Y. Wang, R. R. Zamani, D. Ren, Z. Wang, Y. Xu, D. H. Nam, J. Wicks, B. Chen, X. Wang, M. Luo, M. Graetzel, F. Che, E. H. Sargent and D. Sinton, *Nat. Commun.*, 2021, **12**, 2808.
267 S. Jin, Y. Jeon, M. S. Jeon, J. Shin, Y. Song, S. Kang, J. Bae, S. Cho, J. K. Lee, D. R. Kim and B. K. Cho, *Proc. Natl. Acad. Sci. U. S. A.*, 2021, **118**, e2020552118.
268 H. Luo, J. Qi, M. Zhou, G. Liu, Y. Lu, R. Zhang and C. Zeng, *Bioresour. Technol.*, 2020, **309**, 123322.
269 F. Ammam, P.-L. Tremblay, D. M. Lizak and T. Zhang, *Biotechnol. Biofuels*, 2016, **9**, 163.
270 K. K. Sakimoto, A. B. Wong and P. Yang, *Science*, 2016, **351**, 74–77.
271 H. Liu, T. Song, K. Fei, H. Wang and J. Xie, *Bioresour. Bioprocess.*, 2018, **5**, 7.
272 Y. Hirokawa, Y. Maki, T. Tatsuke and T. Hanai, *Metab. Eng.*, 2016, **34**, 97–103.
273 B. Wang, S. Pugh, D. R. Nielsen, W. Zhang and D. R. Meldrum, *Metab. Eng.*, 2013, **16**, 68–77.
274 K. P. Nevin, S. A. Hensley, A. E. Franks, Z. M. Summers, J. Ou, T. L. Woodard, O. L. Snoeyenbos-West and D. R. Lovley, *Appl. Environ. Microbiol.*, 2011, **77**, 2882–2886.
275 H. Li, P. H. Opgenorth, D. G. Wernick, S. Rogers, T. Y. Wu, W. Higashide, P. Malati, Y. X. Huo, K. M. Cho and J. C. Liao, *Science*, 2012, **335**, 1596.
276 I. Vassilev, P. A. Hernandez, P. Batlle-Vilanova, S. Freguia, J. O. Krömer, J. R. Keller, P. Ledezma and B. Virdis, *ACS Sustainable Tain. Chen. Eng.*, 2018, **6**, 8485–8493.
277 S. Srikanth, D. Singh, K. Vanbroekhoven, D. Pant, M. Kumar, S. K. Puri and S. S.-V. Ramakumar, *Bioresour. Technol.*, 2018, **265**, 45–51.
278 I. S. Yunus, J. Wichmann, R. Wordenweber, K. J. Lauersen, O. Kruse and P. R. Jones, *Metab. Eng.*, 2018, **49**, 201–211.
279 R. K. Yadav, J.-O. Baeg, G. H. Oh, N.-J. Park, K.-J. Kong, J. Kim, D. W. Hwang and S. K. Biswas, *J. Am. Chem. Soc.*, 2012, **134**, 11455–11461.
280 S. Yu, P. Lv, P. Xue, K. Wang, Q. Yang, J. Zhou, M. Wang, L. Wang, B. Chen and T. Tan, *Chem. Eng. J.*, 2021, **420**, 127649.
281 S. Srikanth, M. Maesen, X. Dominguez-Benetton, K. Vanbroekhoven and D. Pant, *Bioresour. Technol.*, 2014, **165**, 350–354.
282 J. Luo, A. S. Meyer, R. V. Mateiu and M. Pinelo, *N. Biotechnol.*, 2015, **32**, 319–327.
283 H.-J. Jo, J.-H. Kim, Y.-N. Kim, P.-W. Seo, C.-Y. Kim, J.-W. Kim, H.-N. Yu, H. Cheon, E. Y. Lee, J.-S. Kim and J.-B. Park, *Green Chem.*, 2022, **24**, 218–226.
284 J. R. Phillips, H. K. Atiyeh, R. S. Tanner, J. R. Torres, J. Saxena, M. R. Wilkins and R. L. Huhnke, *Bioresour. Technol.*, 2015, **190**, 114–121.
285 M. Kopke, C. Mihalcea, F. Liew, J. H. Tizard, M. S. Ali, J. J. Conolly, B. Al-Sinawi and S. D. Simpson, *Appl. Environ. Microbiol.*, 2011, **77**, 5467–5475.
286 C. K. Lim, J. C. Villada, A. Chalifour, M. F. Duran, H. Lu and P. K.-H. Lee, *Front. Microbiol.*, 2019, **10**, 1027.
287 W. F. Liang, L. Y. Cui, J. Y. Cui, K. W. Yu, S. Yang, T. M. Wang, C. G. Guan, C. Zhang and X. H. Xing, *Metab. Eng.*, 2017, **39**, 159–168.
288 T. Schwander, L. Schada von Borzyskowski, S. Burgener, N. S. Cortina and T. J. Erb, *Science*, 2016, **354**, 900–904.
289 T. Cai, H. Sun, J. Qiao, L. Zhu, F. Zhang, J. Zhang, Z. Tang, X. Wei, J. Yang, Q. Yuan, W. Wang, X. Yang, H. Chu, Q. Wang, C. You, H. Ma, Y. Sun, Y. Li, C. Li, H. Jiang, Q. Wang and Y. Ma, *Science*, 2021, **373**, 1523–1527.